# Mouse models in neurological disorders: Applications of non-invasive imaging

Yannic Waerzeggers, Parisa Monfared, Thomas Viel, Alexandra Winkeler, Andreas H. Jacobs

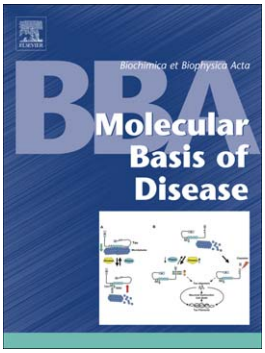


# Mouse models in neurological disorders: Applications of non-invasive imaging

Yannic Waerzeggers, Parisa Monfared, Thomas Viel, Alexandra Winkeler, Andreas H. Jacobs

PII: S0925-4439(10)00088-8
DOI: doi: 10.1016/j.bbadis.2010.04.009
Reference: BBADIS 63096

To appear in: *BBA - Molecular Basis of Disease*

Received date: 14 December 2009
Revised date: 26 April 2010
Accepted date: 29 April 2010

Please cite this article as: Yannic Waerzeggers, Parisa Monfared, Thomas Viel, Alexandra Winkeler, Andreas H. Jacobs, Mouse models in neurological disorders: Applications of non-invasive imaging, *BBA - Molecular Basis of Disease* (2010), doi: 10.1016/j.bbadis.2010.04.009

**22/04/10**

# Mouse models in neurological disorders: applications of non-invasive imaging

Yannic Waerzeggers[1]; Parisa Monfared[1]; Thomas Viel[1]; Alexandra Winkeler[1]; Andreas H. Jacobs[1,2]

[1]Laboratory for Gene Therapy and Molecular Imaging at the Max Planck Institute for Neurological Research with Klaus-Joachim-Zülch Laboratories of the Max Planck Society and the Faculty of Medicine of the University of Cologne, Cologne; [2]European Institute of Molecular Imaging at the University of Muenster, Muenster, Germany

Keywords: neuroimaging, mouse models, neurodegeneration, Parkinson's disease, Alzheimer's disease, neurooncology, glioma

To be submitted to BBA, invited review

**Correspondence:**
Prof. Dr. A.H. Jacobs, MD
Laboratory for Gene Therapy and Molecular Imaging
MPI for Neurological Research
Gleuelerstrasse 50
50931 Cologne
Germany
Phone: ++49 251 83 49300
Fax: ++49 251 83 49313
e-mail: andreas.jacobs@nf.mpg.de

**Abstract**

Neuroimaging techniques represent powerful tools to assess disease-specific cellular, biochemical and molecular processes non-invasively *in vivo*. Besides providing precise anatomical localisation and quantification, the most exciting advantage of non-invasive imaging techniques is the opportunity to investigate the spatial and temporal dynamics of disease-specific functional and molecular events longitudinally in intact living organisms, so called molecular imaging (MI). Combining neuroimaging technologies with *in vivo* models of neurological disorders provides unique opportunities to understand the aetiology and pathophysiology of human neurological disorders. In this way, neuroimaging in mouse models of neurological disorders not only can be used for phenotyping specific diseases and monitoring disease progression but also plays an essential role in the development and evaluation of disease-specific treatment approaches. In this way MI is a key technology in translational research, helping to design improved disease models as well as experimental treatment protocols that may afterwards be implemented into clinical routine. The most widely used imaging modalities in animal models to assess *in vivo* anatomical, functional and molecular events are positron emission tomography (PET), magnetic resonance imaging (MRI) and optical imaging (OI). Here, we review the application of neuroimaging in mouse models of neurodegeneration (Parkinson's disease, PD, and Alzheimer's disease, AD) and brain cancer (glioma).

**Contents**

## 1. Introduction

Over the past years the development of animal models of neurological disorders has progressed rapidly. Neurosciences also increasingly demanded improvements in non-invasive imaging technologies, which could be employed in the assessment of neurological diseases. Especially in the central nervous system non-invasive classification and characterisation of both disease stage and treatment efficacy has become indispensable in the evaluation of established and experimental treatment strategies.

During the past decade, the molecular and genetic causes underlying many neurological disorders have been characterised. Knowledge of the underlying genetic and molecular defects of specific diseases and understanding of related pathophysiological changes are essential for the development of novel efficient therapeutic approaches targeting disease-causing molecular defects. To image molecular and cellular processes in vivo several imaging modalities have been developed and implemented in animal models. Imaging modalities can be roughly divided into two groups: those primarily providing structural information like computed tomography (CT), MRI or ultrasound (US); and those primarily aiming at functional or molecular information, like PET, SPECT or optical imaging (OI). This subdivision, however, is arbitrary and has overlapping boundaries. Some techniques can provide both types of information depending on the imaging settings or administered drugs (e.g targeted or activatable probes). For instance, MRI can not only be used to reveal organ structure and soft tissue morphology, but can also provide functional and metabolic information, such as vascular volume and permeability, tissue perfusion, water diffusion, central nervous system functional activation, metabolic spectroscopy, pH, pharmacokinetics and gene expression. Combining different imaging technologies that merge structural and functional information enables accurate, repetitive, non-invasive disease phenotyping and the measurement of therapeutic outcomes. Furthermore, combining two or more imaging modalities has the potential to exploit the strength and overcome the shortcomings of each modality if used alone. Optical imaging techniques are cost-effective and time-efficient, require less resources and space than PET and MRI and have excellent temporal resolution. However, the common disadvantages of these techniques are the limited spatial resolution and depth penetration, making them only suitable for small animal research, and the lack of optimal quantitative or tomographic information. The nuclear imaging techniques PET and SPECT have a high sensitivity, where very low levels of specific tracer accumulation can be detected but have an inherently limited spatial resolution. MR imaging techniques have a spectacular spatial resolution which is not limited by detector geometry as with nuclear imaging or by tissue scattering properties as by optical imaging, however, temporal resolution is limited and molecular probe detection is several orders of magnitude less sensitive than nuclear imaging techniques.

A multitude of animal models have been established to mimic human disorders. These animal models range from interventional models (such as xenograft, neurotoxic or mechanical lesion models) to knockout and transgenic (mono-, bi- or trigenic through crossbreeding) animals. With the advance of these animal models, non-invasive techniques for the evaluation of disease-associated functional, biochemical and anatomical changes have become indispensable, and a variety of dedicated small animal imaging scanners with high sensitivity, specificity and resolution have been developed. The non-invasive characterization of disease phenotype in mouse models will further increase our understanding of the genetic and molecular alterations associated with disease initiation and progression and will allow the design and evaluation of effective therapeutic interventions. Furthermore, the findings in mouse models obtained by small animal PET/SPECT and MR scanners can be directly

compared to the human situation with clinical scanners and represent true translational research from bench-to-bedside and back to the bench again. However, it should be kept in mind that up till now no true 'humanized' animal models have been developed and that interventional results obtained in mouse models not necessarily will be translated to 100% in the human situation.

## 2. Neurodegeneration

Although no perfect neurodegenerative animal model exist yet, the current models of Parkinson's disease (PD) and Alzheimer's disease (AD) feature complementary aspects of the underlying neurodegenerative processes. These animal models are important in understanding the aetiology, pathophysiology and progression of PD and AD and are essential in the development of therapeutic interventions. In combination with non-invasive neuroimaging techniques they provide a powerful tool to follow the disease process, examine the compensatory mechanisms and investigate the effects of potential treatments preclinically to derive knowledge that will ultimately guide clinical decisions [1].

### 2.1. Parkinson's Disease

#### *2.1.1. Pathophysiology*

Parkinson's disease (PD) is one of the most common neurodegenerative disorders, characterised by clinical symptoms of bradykinesia, resting tremor, rigidity and postural instability. Non-motor symptoms, such as dementia, dysautonomia, olfactory dysfunction and psychiatric features occur frequently, especially in advanced stages of the disease. However, overt PD symptoms only appear when 80% of the striatal dopamine (DA) or 50% of the nigral cells are lost [2] [3]. Thus, the majority of neurodegeneration in PD already occurs before motor dysfunction develops and therefore objective diagnostic methods, such as neuroimaging, are required which can monitor central dopaminergic neuronal loss before the onset of motor symptoms.

PD is characterised by depigmentation and cell loss of neuromelanin-containing cells within the substantia nigra (SN) and other brain stem nuclei. This neuronal loss is associated with Lewy body inclusions in these cells and leads to the fundamental degeneration of the nigrostriatal pathway resulting in DA depletion from the reticular formation (pars compacta) to the striatum, especially the putamen. Later in the disease course, other neurotransmitter systems involving serotonergic cells in the median raphe, noradrenergic cells in the locus ceruleus and cholinergic cells in the nucleus basalis of Meynert also become involved in the neurodegenerative process and are responsible for most of the non-motor symptoms.

The exact aetiology of PD is still unknown; the disease is thought to result from a complex interaction between multiple predisposing genes and environmental exposures [4]. Overall, PD is idiopathic with a subset (<15%) with a family history of PD. An increasing number of loci linked to familial parkinsonism have been found (PARK1-PARK11) [5]. Molecular genetic studies have identified 7 genes associated with these loci. Of these genes, four have been identified to cause autosomal dominant parkinsonism (α-synuclein, *UCHL1*, *NURR1*, *LRRK2*) and three to cause autosomal recessive disease (*DJ-1*, *PINK1*, parkin) [6]. Recessively inherited loss-of-function mutations were found to cause early onset (< 50 years at onset), L-3,4-dihydroxyphenylalanin (L-DOPA)-responsive Parkinsonism. In contrast, dominantly inherited gain-of-function mutations result in more typical, late-onset, Lewy body Parkinsonism with multi-system involvement [7].

#### *2.1.2. Animal models*

Most insights into PD aetiology and pathogenesis come from investigations performed in experimental models of PD. For an extensive overview see [7] [8] [9]. These models aim to

reproduce key pathogenic features of PD including movement disorder induced by progressive loss of dopaminergic neurons in the substrantia nigra and the formation of α-synuclein containing Lewy body inclusions. Experimental PD models can be divided in toxin-induced models and genetic models.

*2.1.2.1. Toxin-induced PD models*

The key neurotoxic models of PD use the toxins 6-hydroxydopamine (6-OHDA), 1-methyl-4-phenyl-1,2,3,6-tetrahydropyridine (MPTP), rotenone, paraquat or epoxomicin.

Historically, 6-OHDA has been introduced as a catecholaminergic neurotoxin more than 30 years ago and has been used essentially in small animals such as rodents. 6-OHDA shares some structural similarities with dopamine and norepinephrine, exhibiting a high affinity for several catecholaminergic plasma membrane transporters such as the dopamine (DAT) and norepinephrine transporters (NET) [8]. Consequently, 6-OHDA can enter both dopaminergic and noradrenergic neurons and inflict damage to the catecholaminergic pathways of both the central and peripheral nervous systems. 6-OHDA destroys catecholaminergic structures by a combined effect of reactive oxygen species (ROS) and quinines [10]. 6-OHDA administration causes nigrostriatal depletion and gliosis when stereotactically injected into the substantia nigra, median forebrain bundle or striatum. However, Lewy body formation has never been convincingly demonstrated in the brain of 6-OHDA-lesioned rats. Unilateral injections result in a typical asymmetric circling motor behaviour whose magnitude in rodents depend on the degree of nigrostriatal lesion and is most prominent after administration of drugs that stimulate dopaminergic receptors such as apomorphine (rotation away from the lesion), or drugs that stimulate the release of dopamine such as amphetamine (rotation toward the lesion). The unilateral 6-OHDA rat model has been and continues to be one of the most popular experimental models of PD when it comes to the preclinical testing of new symptomatic therapies, neuroprotective strategies and transplantation approaches [8].

MPTP is a potent and irreversible mitochondrial complex I inhibitor whose toxic metabolite MPP+ is selectively transported by the dopamine transporter DAT and whose administration results in Parkinsonism. Although dopaminergic neurons in rats are relatively resistant to MPTP-induced toxicity for reasons not clearly understood, in mice susceptibility of the nigrostriatal pathway to neurodegeneration is strain-dependent with C57BL6 mice being more sensitive and Balb/c mice more resistant to MPTP neurotoxicity. Thanks to the MPTP mouse model of PD an enormous body of work regarding the elucidation of the mechanisms of dopaminergic neuron death and the development of experimental neuroprotective therapies has been achieved. Conversely, the monkey MPTP model remains the gold standard for the assessment of novel strategies and agents for the treatment of PD symptoms. It is well established that MPTP produces, in both humans and monkeys, an irreversible and severe parkinsonian syndrome, characterised by all of the cardinal features of PD, including tremor, rigidity, slowness of movement, postural instability and even freezing. However, as for 6-OHDA, Lewy bodies have thus far not been convincingly observed in MPTP-induced Parkinsonism [8].

The herbicide paraquat is structurally similar to MPP+ and is also a mitochondrial complex I inhibitor. However, it is not a substrate or inhibitor of the dopamine transporter DAT. Epidemiological studies have suggested an increased risk for PD due to paraquat exposure, raising the possibility that paraquat could be an environmental parkinsonian toxin [11]. In contrast to 6-OHDA and MPTP, when administered to mice, paraquat also leads to up-regulation and aggregation of α-synuclein [12].

Rotenone is widely used as an insecticide and piscicide and, like MPTP, is highly lipophilic and thus readily gains access to all organs including the brain. In mitochondria, rotenone impairs oxidative phosphorylation and it also inhibits the formation of microtubules from tubulin. Chronic administration of rotenone in rodents can produce a progressive model of Parkinsonism associated with α-synuclein up-regulation and accumulation in Lewy-like pathology [13]. However, despite the use of the exact same regimen of rotenone, the severity of the striatal dopaminergic damage in rats within a given experiment appears highly variable, ranging from none to near complete impairing this model to be used in preclinical neuroprotection studies.

Systemic administration of the proteasomal inhibitor epoxomicin to adult rats has been shown to produce many key features of PD like progressive Parkinsonism which improves with apomorphine treatment, striatal dopamine depletion and dopaminergic cell death with apoptosis and inflammation in the substantia nigra and intracytoplasmic, eosinophilic, α-synuclein/ubiquitin-containing inclusions resembling Lewy bodies [14]. This model promised to be one of the most succesful in recapitulating the progressive movement disorder and pathology associated with PD but has proven very difficult to reproduce. For a more detailed overview on toxin-induced animal models see [8] and [7].

*2.1.2.2 Genetic PD models*

The recent discovery of specific gene mutations causing familial forms of PD has contributed to the development of novel genetic mouse models of PD that provide new tools to implicate and understand the molecular pathways affected in PD. The most common used genetic mouse models of PD are α-synuclein mice, parkin knockout mice, DJ-1knockout mice, Nurr1 and PITX3-aphakia mice.

α-synuclein transgenic mouse lines include α-synuclein knockout mice and mice overexpressing human wild-type, missense mutated (A30P, A53T or A30P+A53T) or truncated α-synuclein under different promoters to target the α-synuclein expression to cells specifically affected by α-synucleinopathies such as the tyrosine hydroxylase promoter for expression in catecholaminergic neurons, the platelet-derived growth factor subunit β (PDGF-β) promoter for pan-neuronal expression or the myelin proteolipid protein promoter for oligodendrocyte expression [15]. These α-synuclein transgenic mouse lines show variable neuropathological and behavioural phenotypes and can be used to study the role of α-synuclein modifications in the course of α-synucleinopathies such as PD, dementia with Lewy bodies and multiple system atrophy characterized by α-synuclein fibrils deposited in neuronal inclusions (Lewy bodies) or in glial cytoplasmic inclusions respectively.

Unlike α-synuclein that has only few identified mutations (A30P, E46K, A53T), more than 100 mutations have been identified in the Parkin gene at the PARK2 locus [16]. Several laboratories have generated Parkin knockout mice by targeting different exons of the Parkin gene. Overall, Parkin knockout mice fail to develop a Parkinsoniam phenotype, but the different knockout models may provide a means to examine the role of Parkin in protein turnover, oxidative stress and mitochondrial dysfunction as Parkin targets proteins for degradation by the proteosome [16].

Also many mutations in the DJ-1 gene at the PARK7 locus have been associated with early onset PD and DJ-1 knockout mice demonstrate decreased motor functions and altered dopamine function in the nigrostriatal pathway.

Both heterozygous Nurr1 and PITX3-aphakia mice are good models for PD because they have the characteristic loss of nigrostriatal DA neurons. However, these models are limited because they do not reproduce the broad pathology seen in PD and only show pathology in the nigrostriatal pathway. Although the DA phenotypes of the α-synuclein, parkin knockout and DJ-1 knockout mice are not as profound as the heterozygous Nurr1 and PITX3-aphakia mice, they may provide insight into the early stages of the disease whereas the heterozygous Nurr1 and PITX3-aphakia mice provide good models to study the later stages of the disease and DA loss which may lead to the development of better symptomatic treatments of PD.

Recent evidence suggests that mitochondrial dysfunction may play a major role in PD. PD patients have an increased number of midbrain DA neurons with respiratory chain deficits compared to non-PD patients and studies of families with rare inherited forms of PD have identified genes involved in regulating mitochondrial function. Manipulation of mitochondrial respiratory genes (e.g. conditional knockout of the gene mitochondrial transcription factor A) in dopaminergic neurons of the midbrain also elicits a PD phenotype in mice (MitoPark mice) with essential features of clinical PD [16]. For a comprehensive overview on genetic mouse models see [9] and [7].

### *2.1.3. Non-invasive phenotyping*

Neuroimaging in PD plays an important role in disease diagnosis and differential diagnosis, in the assessment of disease extent and progression and to determine response to therapy. In the clinical setting, especially MRI and nuclear imaging techniques are applied for the evaluation of PD.

#### *2.1.3.1. MRI*

MRI has been increasingly used to study anatomical or morphological changes (mainly gray matter atrophy) in PD and other neurodegenerative disorders [17] [18]. Furthermore, MRI is being used to map the neurobiological substrate of motor and cognitive symptoms in PD by the use of functional BOLD MRI (blood-oxygen-level dependent MR imaging) [19], and MR spectroscopy (MRS) has revealed decreased N-acetyl-aspartate to creatinine ratios in the striatum of patients with Parkinsonism compared with controls [20].

#### *2.1.3.2. PET*

Over the last decades, especially radionuclide imaging has provided valuable insights into the mechanisms of nigrostriatal degeneration in PD and into the in vivo assessment of disease progression [21]. By using radiolabelled biological substrates involved in DA processing, radionuclide imaging techniques can be applied to assess the pre-synaptic nigrostriatal DA function and integrity [22] as well as the levels and occupancy of the post-synaptic DA receptors by the use of D2-receptor ligands such as [$^{11}$C]-raclopride, [$^{11}$C]- or [$^{18}$F]-labelled spiperone or [$^{123}$I]-iodobenzamide (IBZM). Currently there are three basic approaches to monitor pre-synaptic DA function with PET (**Figure 1**):

1. 6-[$^{18}$F]-fluoro-L-3,4-dihydroxyphenylalanine ([$^{18}$F]-DOPA) PET, regarded as the gold standard for the assessment of presynaptic dopaminergic integrity in vivo. However, the interpretation of [$^{18}$F]-DOPA scans is not straightforward as the measured activity reflects tracer uptake into presynaptic nerve terminals, aromatic amino acid decarboxylase (AADC) activity (decarboxylation of fluoro-dopa to fluoro-dopamine) and the subsequent storage of fluoro-dopamine in synaptic vesicles.
2. DAT imaging using a variety of [$^{18}$F], [$^{123}$I] and [$^{11}$C] labelled antagonists to determine dopamine transporter (DAT) density, e.g. $^{11}$C-d-threomethylphenidate

([$^{11}$C]MP), [$^{123}$I]*N*-ω-fluoropropyl-2β-carbomethoxy-3β-(4-iodophenyl)nortropane ([$^{123}$I]FP-CIT) or 2β-carbomethoxy-3β-(4-[$^{18}$F]-fluorophenyl)tropane ([$^{18}$F]CFT) . DAT is specific for dopaminergic neurons and is responsible for the re-uptake of DA from the synaptic cleft into the pre-synaptic nerve terminal.

3. VMAT2 imaging using [$^{11}$C]-dihydrotetrabenazine (DTBZ) to determine vesicular monoamine transporter type 2 (VMAT2) densitiy. VMAT2 is the protein responsible for pumping monoamines from the cytosol into synaptic vesicles. These synaptic vesicles prevent catabolism of the neurotransmitters and store them for subsequent exocytotic release into the synaptic cleft.

Furthermore, imaging with appropriate radiotracers can also assess cholinergic, serotonergic and opioid function in PD as well as the in vivo distribution of activated microglia ([$^{11}$C]-PK111959) related to PD-associated inflammation. And by labelling ubiquitous molecules such as water ([$^{15}$O]$H_2O$) or glucose ([$^{18}$F]-FDG), the regional cerebral blood flow or global brain metabolism can be assessed.

Mouse models of PD, either genetically modified or toxic, have not been extensively studied with neuroimaging techniques, primarily because of the small size of the mouse brain. Most imaging studies in animal models of PD have been performed in non-human primates (MPTP monkeys) or larger rodents (6-OHDA-lesioned rats). Because the primary neurochemical change in these animal models is the loss of DA-producing cell bodies in the substantia nigra, resulting in greatly decreased levels of striatal DA, most of the imaging studies performed in these animal models focused on investigating aspects of the DA system [1]. In the MPTP model of non-human primates, PET has been used to study the changes in DA metabolism using [$^{18}$F]-DOPA [23-25], the loss of presynaptic DA terminals using DAT tracers such as cocaine analogues [26-28], changes in postsynaptic DA receptors using D2 receptor probes [29-31] as well as general changes in striatal blood flow or oxygen and glucose metabolism [29].

Some recent studies showed the feasibility of microPET to study presynaptic DA function in several mouse models of PD. The tracer most widely used to investigate DA function in PD patients and in MPTP-treated nonhuman primates, [$^{18}$F]-DOPA, can also be used for in vivo imaging in genetic mice models of PD. Sharma and colleagues have shown that striatal [$^{18}$F]-DOPA uptake is reduced in the striatum of homozygous weaver mutant mice compared to both heterozygous and wild-type control mice [32]. In addition, homozygous weaver mutant mice show an age-related decline in striatal [$^{18}$F]-DOPA uptake [33]. It has to be pointed out that [$^{18}$F]-DOPA is an excellent tracer to evaluate the in vivo DA function in humans, non-human primates and mice but cannot be used for in vivo imaging in rats because it does not accumulate significantly in rat striatum [34].

The compensatory changes in the DA system as a result of lost striatal DA innervation, as has been observed in patients with PD, can also be identified by PET in MPTP-lesioned monkeys. In a recent study by Doudet et al. using [$^{11}$C]DTBZ (which binds to VMAT2), [$^{11}$C]methylphenidate (which binds to the DAT) and [$^{18}$F]-DOPA, the authors could show that in the ventral striatum of monkeys that show 80% loss of caudate-putamen DA terminals, the reduction in binding to the DAT (75%) is less severe than the reduction of binding to the VMAT2 or [$^{18}$F]-DOPA uptake (65%) [35]. This suggests that the DAT is downregulated after the loss of DA innervation, presumably to reduce reuptake and enhance synaptic levels of DA, and is consistent with human PET studies in early PD patients [36]. Even in asymptomatic monkeys, compensation appears to occur after MPTP treatment, since normal levels of striatal [$^{18}$F]-DOPA uptake are maintained in the face of significant reductions in the

number of tyrosine hydroxylase positive (TH+) neurons in the SN [37]. Thus, the impressive capacity of the nigrostriatal DA system for compensation, as suggested by the observation that a loss of approximately half of nigral DA neurons is required to observe symptoms of PD [2], is also reflected in the MPTP-treated nonhuman primate model. Furthermore, the observation that the dysfunction of the DA system can be measured in MPTP-treated nonhuman primates that not yet show overt behavioural symptoms (presymptomatic phase) suggest that PET could provide a method to identify, measure, and follow disease biomarkers in preclinical studies of neuroprotective interventions [26, 30, 38-40].

Similar to MPTP lesions in non-human primates, unilateral 6-OHDA lesions of the nigrostriatal projections (medial forebrain bundle, MFB) in rats result in decreased [$^{11}$C]CFT binding to the DAT and decreased [$^{11}$C]DTBZ binding to the VMAT2 as a result of decreased density of the transporter and loss of presynaptic DA terminals [41] and an increased [$^{11}$C]raclopride binding to D2 receptors due to upregulation of these receptors [42, 43]. Furthermore, it could be shown that there is a dose-dependent relationship between the amount of 6-OHDA injected into the MFB and PET measures of the integrity of the striatal DA system [1, 41]. In contrast to the traditional MFB lesion model, which leads to near-complete loss of DA innervations in the lesioned hemisphere, partial lesions can be accomplished through the intrastriatal infusion of 6-OHDA. Unilateral striatal infusion of 6-OHDA decreases striatal [$^{11}$C]CFT binding and increases [$^{11}$C]PK11195 binding, a ligand of peripheral benzodiazepine receptors and a surrogate marker of reactive microglia, in the lesioned striatum, at three weeks post-lesion compared to baseline [44]. In the same model, daily treatment with a COX-2 inhibitor has been shown to prevent striatal microglial activation at 12 days postlesion, without preventing DA terminal loss [45].

Also pharmacological MRI has been used to detect changes in the 6-OHDA rat model after amphetamine or apomorphine administration and gives insights into the physiological effects that underlie the behavioural response [46, 47]. Lauwers et al. evaluated by behavioural testing and non-invasive imaging of DAT activity the phenotypic effects of local overexpression of α-synuclein in the substantia nigra of rats [48]. Lentiviral vector-induced overexpression of the A30P clinical mutant of α-synuclein let to a dose-dependent motor dysfunction (amphetamine-induced asymmetric rotation) with considerable inter-individual variations. In those rats exhibiting more than 100 ipsiversive rotations, the underlying deficits in dopaminergic neurotransmission could also be monitored non-invasively by means of [$^{123}$I]FP-CIT ([$^{123}$I]*N*-ω-fluoropropyl-2b-carbomethoxy-3b-(4-iodophenyl)nortropane) SPECT (DaTSCAN). LV-SYN(A30P)-transduced rats showed up to 31% reduction in dopamine transporter binding (mean 10±15%, $p<0.05$) compared to normal rats, whereas in the positive control rats (6-OHDA rats) an average loss of 94±13% dopamine transporter activity could be monitored.

### *2.1.4. Therapy*

Therapy of PD is mainly based on pharmacological treatment with symptom-reducing or neuroprotective drugs. Pharmacological dopamine replacement using oral L-DOPA has been over many years the treatment of choice. However, even if the symptomatic benefits of oral L-DOPA are remarkable in the early stages of the disease, with time the majority of PD patients develop motor complications such as marked swings between immobility and mobility (on–off motor fluctuations), involuntary movements (dyskinesia), and neuropsychiatric complications [49]. Therefore, considerable efforts have been made to develop novel treatment approaches that provide antiparkinsonian benefits without side effects and new forms of therapy are emerging, including deep brain stimulation as well as gene- and cell based therapies. Evaluation of therapeutic efficacy has usually been limited to clinical scores, such as the Unified Parkinson Disease Rating Scale (UPDRS). However, over the last years the targets for potential disease modifying treatments have been more and more

approached by in vivo neuroimaging techniques. Several preclinical and clinical trials testing antiparkinsonian or neuroprotective drugs have utilised PET or SPECT imaging to non-invasively assess disease progression in PD [50] [51] [52].

*2.1.4.1. Gene therapy*

Gene therapy for PD was first developed in rat models using transduction of a single gene encoding tyrosine hydroxylase (TH), the enzyme that converts tyrosine into L-dopa. In the past ten years, gene therapy approaches for PD have been further developed into three directions: (i) transduction of multiple genes essential in the production of dopamine and dopamine turnover in nigro-striatal nerve terminals, (ii) transduction of genes encoding growth and antiapoptotic factors for the prevention of further degeneration of nigrostriatal neurons, (iii) vector and promoter systems which are non-toxic and support long-lasting gene expression. For a comprehensive overview on gene therapy approaches in neurodegenerative disorders see Jacobs et al [53].

In a recent study, the correction of dopaminergic neurotransmission after gene therapy could be demonstrated with [$^{11}$C]-raclopride PET imaging and correlated to the behavioural recovery [54]. In this study local delivery of an adeno-associated viral vector coexpressing the tyrosine hydroxylase (TH) and GTP cyclohydrolase 1 (GCH1) enzymes in the striatum of rats with a unilateral 6-OHDA lesion of the nigrostriatal projection neurons resulted in reconstitution of the DOPA synthesis capacity in the denervated striatum, and led to recovery of motor functions in the treated animals. Furthermore, the presence of endogenous DA at the striatal D2 receptor sites could be monitored non invasively with the [$^{11}$C]raclopride tracer and microPET imaging *in vivo* as evidenced by normalization of the increased [$^{11}$C]raclopride binding in the hemiparkinsonian rats. In the same study the authors quantified separately D2 receptor density and affinity *in vivo* and *in vitro* and confirmed that the changes in [$^{11}$C]raclopride binding observed are explained by a change in the apparent affinity and not by a change in D2 receptor density.

Neuroprotective strategies may be especially useful in early PD stages and neurotrophic factors have attracted considerable interest as potential therapeutic agents in PD. It has been shown that glial cell-derived neurotrophic factor (GDNF; [55]) and brain cell-derived neurotrophic factor (BDNF; [56]), as well as other neurotrophic factors related to GDNF, such as neurturin, can protect nigrostriatal neurons from neurotoxic stress and can promote regeneration in rat and primate models of PD [57] [58] [59] [60] [61]. In MPTP-treated baboons, intracerebroventricular implantation of cells genetically engineered to release GDNF attenuates the loss of [$^{18}$F]-DOPA uptake within the caudate (the region closest to the site of the cell transplant) [62], whereas lentiviral delivery of GDNF into the lesioned striatum and substantia nigra one week after unilateral MPTP treatment in non human primates reverses behavioural changes, enhances striatal [$^{18}$F]-DOPA uptake compared to controls and prevents nigrostriatal degeneration [59]. In the unilateral 6-OHDA model of PD in rats, GDNF infusion into the SN and lateral ventricle protects against loss of TH+ cells in the SN and prevents the 6-OHDA-induced reduction in DAT as measured by [$^{11}$C]RTI-121 [63, 64].

*2.1.4.2. Cell therapy*

The loss of a specific type of dopaminergic cells in PD makes the prospect of replacing the missing or damaged cells very attractive. Several cell replacement strategies have been tested under experimental and clinical conditions in parkinsonian animal models and advanced PD patients [65]. In animal models cell types used are mouse or non-human primate embryonic stem cells [66] [67] [68], rodent or human embryonic/fetal/adult tissue-specific neural stem cells [69] [70]. Several clinical trials have been performed with retinal pigmented epithelial cells on gelatine beads (Spheramine®) [71] or primary human embryonic/fetal mesencephalic

tissue [72] [73] transplanted into the striatum of PD patients. To ensure the best clinical outcome, cell transplantation therapies can easily be perfected in preclinical animal models.
In recent years much progress has been encountered in non invasive detection of transplanted cell location and function with MRI [74] but also PET imaging can be used to evaluate transplant function [75]. Striatal transplantation of fetal DA neurons in unilateratl 6-OHDA rats restores the rCBV response to amphetamine as measured with phMRI as well as the [$^{11}$C]CFT binding in the lesioned striatum and behavioural recovery does not occur until [$^{11}$C]CFT binding is restored 75-85% of the intact side [76, 77]. In the same animal model, Bjorklund and colleagues have shown that mouse ES cells transplanted into the rat striatum differentiate into DA neurons and decrease behavioural asymmetries (drug-induced rotation). In addition, [$^{11}$C]CFT binding was increased in the grafted striatum and correlated with the number of TH+ neurons in the graft, and amphetamine-induced increases in rCBV in the corticostriatal pathway were restored to control levels, as measured by MRI [66].

## 2.2. Alzheimer's Disease

### *2.2.1. Pathophysiology*

Alzheimers's disease (AD) is the most common form of dementia in the elderly comprising more than 50% of all dementia cases and the risk of developing AD doubles approximately every 5 years between the ages of 65 and 85 years. AD is characterised by early memory deficits, followed by the gradual erosion of other cognitive functions. The hallmark pathological features of AD in the human brain comprise intracellular neurofibrillary tangles (NFT), extracellular amyloid depositions in the form of senile plaques and blood vessel deposits, synapse dysfunction and synaptic loss, neuronal loss, increased oxidative damage to lipids, proteins and nucleic acids and loss of biometal homeostasis. These histopathological features presumably all lead to another key pathological signature of AD: brain atrophy. The major constituents of the amyloid plaques are insoluble fibrils of the amyloid-beta (Aß) peptides, generated by proteolytic processing of the larger amyloid precursor protein (APP) that is found normally in cell membranes and membranes of intracellular organelles by two proteases, the ß- and γ-secretases [78]. Aß fragments of variable lengths, in particular the 40- and 42-amino-acid subspecies (Aß 40 and Aß 42), are major constituents of amyloid plaques [78] [79]. The NFT represent insoluble polymers of hyperphosphorylated tau protein that in its normal phosphorylated state stabilizes microtubules of axonal cytoskeleton. The most severe neuropathological changes occur in the hippocampus, followed by the association cortices and subcortical structures, including the amygdala and the nucleus basilis of Meynert. The progression of these pathological processes is associated with the cognitive decline characteristic of AD and probably develops many years before the clinical manifestations of the disease become apparent.

The cause of AD remains controversial. Recently, the apolipoprotein E gene on chromosome 19 has emerged as a susceptibility gene for sporadic AD (SAD) and a putative marker for AD with the apoE4 allele increasing and the apoE2 allele decreasing the risk of developing AD. The apoE4 allele has a role in the accumulation of Aß42 and its binding properties to tau, and it operates as a risk modifier by decreasing the age of onset in a dose-dependent manner [80]. And although ß-amyloid has been suggested as the primary cause of AD [81], it is still under debate which specific form of Aß is responsible for the neuronal damage leading to the cognitive impairment in patients. It is still an open question whether soluble or insoluble Aß oligomers or mature amyloid are most toxic [82]. These facts necessitate the attempt for in vivo detection and quantification of amyloid in the brain of patients during the course of the disease to understand the natural history of the disease and to evaluate the effects of antiamyloid therapies.

In families with early-onset AD (FAD) autosomal dominant mutations have been identified in three genes, i.e. presenilin (PS-) 1 and 2 and amyloid precursor protein (APP) genes. FAD accounts for less than 1% of the total number of AD cases. Mutations in these genes alter normal processing of APP causing the extracellular accumulation of amyloid plaques. Most FAD cases are caused by mutations in the genes for PS-1 and PS-2, of which over 130 have been identified. The presenilins are components of the proteolytic γ-secretase complex that, together with ß-secretase, generates Aß. Also more than 20 pathogenic mutations have been identified in the gene for APP. Other than age of onset, the clinical and pathophysiological features of early-onset FAD cannot be discriminated from those of late-onset SAD. Although no mutations in the gene encoding tau (MAPT) have been identified in AD patients, both exonic and intronic mutations in MAPT have been found in patients with other forms of dementia, such as frontotemporal dementia and Parkinsonism [83, 84].

### *2.2.2. Animal models*

Mouse models of AD have become essential biosystems for developing and defining optimal imaging approaches to visualise AD pathology in vivo as well as for understanding the genotype-phenotype interaction in this disease. Very few studies have attempted to model AD in non-human primates and rats using excitotoxic lesions in specific brain areas such as perirhinal and entorhinal cortices or hippocampus and to monitor the induced pathological features with [$^{18}$F]-FDG PET (decreased cortical and hippocampal glucose metabolism) [85] [86] or MRI (decreased BOLD signal in hippocampus and cortex or increased apparent diffusion coefficients (ADCs) in the CA1 region) [87, 88].

The most common rodent model of AD is the transgenic mouse model. The finding that, in familial forms of dementia, the genes that encode the proteins that are deposited in plaques and NFT (Aß and tau, respectively) are mutated suggested a causal role for these proteins in the disease process and led to the generation of transgenic animal models. There exist multiple transgenic dementia mouse models (tau models, Aß models, secretase models, ApoE models and axonal transport models) and some emphasize only one hallmark pathological AD feature, while double or triple transgenic models develop more clinically relevant pathology. Typical transgenic (tg) mouse models of AD mimic various aspects of AD such as over-expression of human amyloid precursor protein (hAPP), presenilin-1 or -2 or apo-lipoprotein E and several excellent recent reviews exist [89] [90]. Most of these murine models of AD typically show overexpression of hAPP and sufficient Aß levels to insure amyloid deposition. Besides being useful tools in the analysis, understanding and possible treatment of the disease based on findings in histology, biochemistry, molecular biology and behavioural testing these mouse models have been of help in characterisation of amyloid-imaging agents and have been used for non-invasive phenotyping by multi-tracer PET and MRI.

### *2.2.3. Non-invasive phenotyping*

To date, there is no definitive pre-mortem diagnosis for AD in patients. As the NFT and ß-amyloid plaques are the neuropathological hallmarks of AD that preclude the cognitive decline, the ability to directly visualise these pathologies with in vivo diagnostic imaging techniques might contribute to the early diagnosis and monitor the success of treatments. Furthermore, imaging in animals may provide a tool to non-invasively monitor pathological changes and correlate these with behavioural changes.

#### *2.2.3.1. PET*

The development of PET amyloid ligands based on radiolabelled analogues of Congo red and thioflavin started more than 10 years ago and went from in vitro binding studies in tissue homogenates in mice or human autopsy brain tissues to imaging studies in rodents, humans and non-human primates. Direct imaging of ß-amyloid plaques in transgenic mouse models

has been mainly performed using the compound N-methyl-[$^{11}$C]2-(4'-methyl-aminophenyl)-6-hydroxybenzothiazole (or [$^{11}$C]PIB for "Pittsburgh Compound-B") that binds fibrillary (but not amorphous) Aß deposits at low nanomolar affinity, readily passages the blood-brain barrier and rapidly clears from normal brain tissue [91]. Toyama and colleagues [92] used the Tg2576 mouse model of Alzheimer's disease to evaluate the feasibility of microPET imaging using the radiolabeled compound [$^{11}$C]PIB to image and quantify Aß plaques in vivo. Surprisingly, unlike in humans and aged non-human primates, the tracer [$^{11}$C]PIB does not accumulate to a great extent in the APP transgenic mouse brain in vivo [93] although multiphoton imaging in transgenic mice overexpressing APP has shown that PIB after peripheral administration enters the brain quickly and labels Aß deposits [94]. A possible reason for the insensitivity of PET imaging in capturing mouse amyloid with [$^{11}$C]PIB may lie in the paucity of high-affinity binding sites for this radioligand in APP Tg mouse brain compared with AD brains and can be overcome by administering [$^{11}$C]PIB synthesized with high specific radioactivity [95].

Besides the direct measurement of ß-amyloid plaques, microPET imaging can help in the characterisation and phenotyping of animal models of Alzheimer's disease by taking advantage of other radiotracers already implemented in the clinical application for diagnosis in AD like e.g. [$^{18}$F]FDG (glucose hypometabolism), [$^{11}$C]*N*-methyl-4-piperidyl-acetate ([$^{11}$C]MP4A, attenuated cholinesterase activity) or [$^{11}$C]flumazenil ([$^{11}$C]FMZ, neuronal integrity). Considering that [$^{18}$F]FDG PET is becoming one of the most widely used diagnostic tools for clinical AD, the expectation that this technique would also be widely used in examining transgenic mice has not been met [1]. This is most likely a result of the limited resolution of PET, because whereas autoradiographic studies show decreased cerebral glucose metabolism in the posterior cingulate cortex, in vivo PET imaging does not allow the identification of this change [96]. To combat the spatial resolution limitations of PET, multimodal imaging approaches combining highfield-strength MRI with microPET imaging are increasingly being performed. In a knock-out mouse model for the brain/neuron specific insulin receptor (NIRKO) Schubert et al. [97] investigated the influence of neuronal insulin resistance in neurodegeneration and could demonstrate reduced Akt and GSK3ß phosphorylation and hyperphosphorylation of Tau protein in NIRKO mice as compared to controls. Speculations on the regulative role of neuronal insulin receptors on cerebral glucose metabolism lead to the performance of microPET analyses in NIRKO mice *in vivo* with [$^{18}$F]FDG in collaboration with our group. In this study, tg and control animals underwent [$^{18}$F]FDG PET as well as *in vivo* high-resolution microMRI for co-registration aspects to differentiate distinct brain regions and hypermetabolic active harderian glands and to ensure proper region-of-interest (ROI) analysis. Brain-to-background ratios for [$^{18}$F]FDG uptake in NIRKO mice did not show any significant difference as compared to control animals suggesting that in this specific study insulin signalling did not have a substantial influence on basal brain glucose metabolism detectable by microPET (**Figure 2**). In a subsequent study, including multi-tracer PET imaging, the effect of locus ceruleus (LC) degeneration (induced by N-(2-chloroethyl)-N-ethyl-bromo-benzylamine (dsp4) that specifically targets the noradrenergic neurons of the LC) and its contribution to AD pathogenesis was investigated in a Tg AD mouse model (APP23 transgenic mice) [98]. In this study only transgenic mice who were also treated with dsp4 showed decreased cortex/cerebellum ratios in [$^{18}$F]FDG uptake, [$^{11}$C]FMZ binding, and [$^{11}$C]MP4A trapping, indicating that locus ceruleus degeneration and inflammatory reactions contribute significantly to AD pathogenesis (**Figure 3**).

*2.2.3.2. MRI*

By far, the most commonly employed imaging technique in Tg mouse models of AD is MRI. MRI has been used both clinically and preclinically to provide secondary structural readouts such as measures of brain atrophy or indicators of microstructural changes of brain

parenchyma [99]. Brain atrophy can be assessed by measurements of total or partial brain volume (e.g. hippocampal volume) or indirectly by measuring ventricular volumes. In 24-months old hAPP23 mice ventricles are enlarged by 18±4% compared with wild type littermates. Microstructural changes in brain parenchyma can be measured by ADC, a sensitive indicator of alterations in cellular volumes, and was evident only in 24-months old transgenic mice [100]. And diffusion tensor imaging (DTI) may give more detailed information about the type of diffusion abnormality based on the directional compounds. For instance, DTI of the white matter tracts in APPSW mice demonstrated that young APPSW mice were comparable to control mice, whereas aged mice had a reduction in relative anisotropy in all white matter tracts compared with age-matched controls [101].
However, the prominent role of MRI in preclinical AD research arises primarily from the fact that ß-amyloid deposits contain iron allowing them to be directly detectable by MRI in T2-weighted or T2*-weighted images as hypointense areas in high-resolution images [102] [103] [104]. Even individual amyloid plaques throughout the cerebral cortex and hippocampus using T2-weighted pulse sequences can be detected [105]. Nevertheless, T2*-weighted hypointensities alone are not specific for AD and other sources of T2/T2*-weighted hypointensities (such as blood vessels) or variability in plaque metal content may lead to misidentification [106] [103] [104]. Therefore, the more specific approach for the early detection of AD is the use of targeted contrast agents [107]. A first approach uses an Aß peptide component that specifically binds to plaques and that can be labelled with either gadolinium or dextran-coated ultrasmall superparamagnetic iron oxide nanoparticles for direct amyloid plaque detection in vivo by T1-weighted or T2-weighted MRI respectively [108] [109]. A second approach uses an anti-Aß monoclonal antibody fragment attached to a gadolinium chelator [110]. Also a fluorinated amyloidophilic compound based on Congo-red, (E,E)-1-fluoro-2,5-bis(3-hydroxycarbonyl-4-hydroxy)styrylbenzene (FSB), and detectable by both $^{1}H$ and $^{19}F$ MRI has recently been reported to target plaques [111].
$^{1}H$-MRS has been proposed as a sensitive tool to detect neurodegenerative processes, in particular AD. The analysis is primarily based on two signals: myo-inositol (an indicator of membrane and second messenger turnover) and *N*-acetylaspartate (NAA, a marker of neuronal integrity). Patients with MCI have MRS spectra with an increased myo-inositol signal intensity whereas AD patients have an additional significant decrease in the NAA peak [112]. However, in PS2APP transgenic mice only in aged animals (24 months) significant decreases of the NAA and glutamate signals can be observed, at younger age there are no differences between tg and wt littermates [113].
Functional MR imaging has also been used in AD models. The cerebral haemodynamic response induced after pharmacological stimulation with a GABA antagonist or after electrical forepaw stimulation and measured with functional MRI could only reveal reduced responsiveness in aged APP23 mice [114] [115].

### *2.2.4. Therapy*

To date, there is no cure for AD and the available clinical core treatment is only symptomatic and based on pharmacological therapy [116]. However, animal models are playing a central role in the development of effective therapeutic strategies based on current knowledge of the biological mechanisms underlying the disease and several clinical trials are on their way.

#### *2.2.4.1. Drug treatment*

Several drugs have proven to be of use in the stabilisation/reduction of the cognitive and functional decline during various stages of the disease. Cholinesterase inhibitors (rivastigmine, donepezil and galantamine) are the standard first-line therapy in patients with mild-to-moderate AD. The N-methyl-D-aspartate (NMDA) receptor antagonist memantine is used as mono-therapy or in combination with a cholinesterase inhibitor for patients with

moderate AD, and as mono-therapy for patients with severe AD. Those drugs are the only drugs approved by the United States Food and Drug Administration (FDA) for the treatment of AD and augment cholinergic transmission or reduce glutamate-mediated neurotoxicity associated with the disease.

*2.2.4.2. Experimental treatment*

Other, more experimental treatment approaches address the pathological mechanisms of the disease (Aß deposits, NFT, oxidative stress and neuronal loss). Vaccination was the first treatment approach demonstrated to have a genuine impact on amyloid plaque load and disease process, at least in animal models of AD [117]. Several studies evaluated the therapeutic potential of active immunisation by vaccination with Aß homologous peptides [118] [119] [120] or passive transfer of exogenous anti-Aß monoclonal serum [121] [122] in Tg mice models of AD and the effects of such anti-amyloid treatment on amyloid burden have been monitored with non-invasive imaging techniques such as [$^{11}$C]PIB PET [95]. Although active immunisation with synthetic Aß1-42 has been shown to be effective in mouse models to significantly reduce the Aß burden accompanied by improved cognitive performance, clinical trials had to be stopped after enrolment of about 300 patients due to the development of an extensive T-cell mediated aseptic meningoencephalitis in 6 % of treated patients [123] [124]. Clinical trials for passive immunisation are underway.

A number of proteins actively promote the conformational transformation and stabilisation of soluble Aß to fibrillary Aß and are called pathological chaperones. Such proteins in AD are apolipoprotein E, especially its ε4 form, α1-antichymotrypsin (ACT) or C1q complement factor. Other proteins or compounds such as Congo red, anthracycline, rifampicin, anionic sulphonates or melatonin can interact with Aß and prevent its aggregation into fibrils or bind to Aß and break the formation of ß-sheet structure (ß-sheet breakers). Due to their action these compounds have been tested in experimental approaches [125] [126].

The progressive neuronal loss in AD has been the target of nerve growth factor (NGF) therapy [127] [128]. Neurotrophic factors support neuronal survival, migration and neuritic outgrowth, support the fully functional state of mature neurons and can exert direct effects on synapse function influencing neurotransmitter release and synaptic efficacy [129] [130]. First animal studies showed that intracerebroventricular infusion of NGF can prevent the degeneration of cholinergic neurons in rodent and primate models of cholinergic neuronal degeneration [131] [132] but also causes numerous side effects like weight loss [133], sympathetic axon sprouting [134] and Schwann cell migration [135]. Similar adverse effects were encountered after intracerebroventricular infusion of recombinant NGF in patients with AD [136] and therefore other delivery approaches had to be developed.

In recent years gene delivery has emerged as a potent technique for chronic delivery of therapeutic proteins of interest in vivo. CNS gene delivery can be achieved *ex vivo* (injection of autologous cultured cells genetically modified to produce NGF in the region of the cholinergic basal forebrain (experimental: [137] [138] [139], clinical: [140]) or in vivo (direct injection of viral vectors carrying the NGF gene into the basal forebrain region which then becomes genetically modified to produce elevated levels of NGF (experimental: [141] [142], clinical: [143]).

Lately, also dietary strategies have gained increased recognition in preventing AD. Not only intermittent fasting and caloric restriction diets but also diets enriched in omega-3 polyunsaturated fatty acids or the antioxidants resveratrol, Ginkgo biloba or the green tea component epigallocatechin-3 and moderate consumption of red wine have shown to reduce Aß neuropathology and/or the memory impairments in Tg mice [144] [145] [146] [147] [148] [149].

Finally, biometals have been implicated in AD neuropathology and a detailed review on the loss of metal homeostasis in AD and the modulation of metal bio-availability as a therapeutic strategy for the treatment of AD has been published by Crouch et al. [150].

## 3. Neurooncology

Normal brain is composed of a variety of cell types, including neurons, glia (astrocytes, oligodendrocytes, microglia and ependymal cells), vascular epithelium and meningeal cells. Intracranial tumours arising from brain meninges (meningiomas) and tumour metastases from systemic cancer (such as lung, breast, colon) are not considered primary brain tumours. Primary brain tumours can be classified into gliomas, occurring in the brain parenchyma above the tentorium, and medulloblastomas, child or young adult cerebellar tumours occurring below the tentorium. Here we will focus on gliomas.

### *3.1. Pathophysiology*

Diffuse infiltrative gliomas are the most common primary adult brain tumour, accounting for 40% of all primary and 78% of all malignant central nervous system tumours. The term glioma includes several heterogeneous entities, which have in common a presumed glial cell of origin. Subcategories of gliomas include astrocytomas, oligodendrogliomas, oligo-astrocytomas, ependymomas and glioblastomas. According to the World Health Organisation (WHO) classification, gliomas receive a histopathologic grade on the basis of the presence of nuclear changes, mitotic activity, presence of endothelial proliferation and necrosis [151]. Low grade gliomas (WHO II) are defined as diffusely infiltrative astrocytotic tumours with cytological atypia (diffuse astrocytomas, juvenile pilocytic astrocytomas, oligodendrogliomas, gangliogliomas and mixed gliomas); tumours presenting anaplastic cell types and high mitotic activity are classified as WHO III (anaplastic forms of astrocytoma, oligodendroglioma and oligastrocytoma); gliomas with additional microvascular proliferation and/or necrosis as WHO grade IV (glioblastoma and its variants). The histological grading is highly relevant to predict prognosis. The median survival of patients with WHO grade II glioma is usually more than 5 years whereas the median survival of patients with high grade gliomas remain modest (< 15 months) despite recent advances in microsurgical techniques, radiation and chemotherapy [152]. Surgical resection and radiotherapy have been the mainstay of treatment [153] and only recently have the benefits of chemotherapy been unequivocally shown in a randomized trial [154]. Yet, even under such therapies, recurrence is the norm, and disease will follow a fatal course in virtually all patients with malignant glioma. This inability to successfully treat brain tumours mostly is due to the lack of understanding the underlying complex brain tumour biology and treatment outcome is hardly predictable because of high genetic heterogeneity and individually different molecular tumour phenotypes that are responsible for tumour growth.

Glioblastoma may arise through 2 distinct pathways of neoplastic progression. Tumours that progress from lower grade (II or III) astrocytic tumours are termed secondary or type 1 GBM; tumours that arise de novo without any evidence of a lower-grade precursor are termed primary or type 2 GBM. Secondary GBM develop in younger patients (fifth to sixth decade) with time to progression from low-grade lesions ranging from months to decades. Primary GBM develop in older individuals (sixth to seventh decade) and have short clinical histories (less than 3 months).

Over the past two decades a complex series of molecular changes leading to glioma development have been identified. Investigations into glioma pathogenesis have revealed several disturbances in key biological pathways resulting in de-regulation of the cell cycle, alterations of apoptosis and cell differentiation, in neovascularization as well as tumour cell

migration and invasion into brain parenchyma. These highly complex signal transduction cascades, which are differentially activated and silenced, involve signalling between multiple parallel and interrelated pathways (**Figure 4**). Growth factors and their receptors, such as epidermal growth factor receptor (EGFR), vascular endothelial growth factor (VEGF), platelet-derived growth factor receptor (PDGFR) and transforming growth factor-β, primarly acting through receptor tyrosine kinases (RTK), have been implicated in the initiation and progression of gliomas [155, 156]. EGFR amplification occurs in ~40% of GBM and a constitutively active deletion mutant, EGFRvIII, is found in 20-30% of GBM.

Also disruptions of a set of tumour suppressor pathways with direct effects on cell cycle control are involved in glioma pathogenesis. These genetic alterations include a loss, mutation or hypermethylation of tumour suppressor genes (such as TP53) and other genes involved in the regulation of the cell cycle (such as cyclin-dependent kinase inhibitor 2A CDKN2A (also known as INK4a/ARF locus), $p16^{INK4a}$, $p14^{ARF}$ and phosphatase and tensin homology (PTEN)) as well as activation or amplification of oncogenes (such as MDM2, cyclin-dependent kinase 4 CDK4 and cyclin D1 and D3), inactivation of the retinoblastoma (Rb) tumour suppressor pathway, loss of heterozygosity (LOH) on chromosome 9p, 17p, 22q, 13q, 19q or 10q and O6-methylguanine-DNA-methyltransferase (MGMT) promoter methylation [156, 157]. During progression from low-grade astrocytoma (WHO grade II) to anaplastic astrocytoma (WHO grade III) and to glioblastoma multiforme (WHO grade IV) a step-wise accumulation of these genetic alterations occurs and distinct molecular genetic alterations have been identified in primary and secondary GBM [158] [159]. Primary GBM are characterised by relative high frequencies of EGFR amplification, PTEN deletion, CDKN2A/p16 loss, pRb alteration and LOH 10p and 10q, whereas secondary GBMs often contain *TP53* mutations or G:C→A:T mutations at CpG sites. Furthermore, molecular alterations have been identified, which indicate therapeutic response of patients and, thus, have prognostic relevance [160-163].

### *3.2. Animal models*

Many in vitro and *in vivo* models of brain tumours have been developed and they increased our understanding of brain tumour initiation, formation, progression and metastasis and provided an experimental system to discover novel therapeutic targets and test various therapeutic agents. Many tumour-derived cell lines have been established and they are often employed for screening of novel drugs in cell culture or xenograft experiments because of their ready availability and ease of use [164]. Xenograft models, induced either by subcutaneous or by orthotopic (into native tumour sites) injection of primary tumour cells or tumour cell lines, represent the most frequent used in vivo cancer modelling system. However, both cell culture and xenograft model systems lack the stepwise genetic alterations thought to occur during tumour progression and do not recapitulate the genetic and cellular heterogeneity of primary tumours and the complex tumour-stroma interaction. In contrast, genetically engineered mouse models recapitulate more accurately the causal genetic events and subsequent molecular evolution in situ and give rise to tumour-stroma interactions resembling those of the native tumours and also harbour cellular subpopulations like cancer stem cells thought to be of central importance to the development, maintenance and drug resistance of brain cancer [164]. In recent years, several such mouse models have been developed using combinations of the above-mentioned glioma-associated genetic alterations. For review see [165] [166] [167].

Most of the cell lines used in xenograft cancer models are transgenic cell lines that exhibits overexpression, underexpression or complete inactivation of a gene of interest to provide insights in the molecular and functional characteristics of cancer. Moreover, in addition to this gene of interest often a second reporter gene is introduced and allows for non-invasive

phenotyping of the effects of induced molecular alterations by molecular imaging techniques [168].

### *3.3. Non-invasive phenotyping*

The imaging techniques that are used clinically to evaluate patients with primary and metastatic brain tumours are also commonly employed in mouse brain tumour models and allow the early identification of morphological, pathophysiological, functional and metabolic changes associated with tumour growth.

#### *3.3.1. MRI*

Conventional MRI techniques, such as T1- and T2-weighted imaging, contrast-enhanced T1-weighted imaging, dynamic contrast enhanced (DCE) imaging and diffusion-weighted imaging (DWI) provide information on tumour localisation and extent, local blood-brain barrier (BBB) damage and brain invasiveness, regional blood flow and blood volume and tumour cellularity which, in the clinical setting, are known to be associated with glioma grade and prognosis. Also secondary changes associated with tumour growth, such as oedema, brain shift or hydrocephalus can be determined on two- or tri-dimensional MR images. Recently, McConville et al. demonstrated that MRI can be used to predict tumour grade and survival in a genetically engineered mouse model of glioma [169]. In the Ntv-a model, approximately 100% of mice spontaneously develop gliomas by 3 weeks of age, with 30% of these tumours displaying high-grade histologic features. T2-weighted and T1-weighted, gadolinium-enhanced MRI could distinguish between high- and low-grade tumours on the basis of their growth rate and contrast enhancement.

However, care should be taken when interpreting contrast leakage as an indicator of BBB breakdown due to malignant degeneration as this sign can be absent in diffuse infiltrative tumour regions, non-specific or induced by therapeutic intervention [170]. Especially the treatment with antiangiogenic compounds can restore the BBB in angiogenic regions without concomitant tumour regression and underlines the need for alternatives to gadolinium-based contrast-enhanced MRI to detect progressing tumour portions that are not associated with angiogenesis and thus BBB disruption but are based on an angiogenesis-independent tumour growth, for instance via cooption of preexistent vasculature [171]. Although these infiltrative lesions can not be detected with gadolinium-based contrast enhanced MRI, the relatively low vascular volume in these tumours, as compared to the surrounding tissue, can be exploited to detect these lesions using blood pool contrast agents such as ultrasmall particles of iron oxide (USPIO) [172] and to evaluate the response to antiangiogenic therapy [173].

Another technique to follow in vivo tumour angiogenesis as a necessary component of tumour expansion, invasion and possible metastasis is DCE MRI that enables the longitudinal investigation of changes in tumour vascular permeability, vascular density and vessel morphology. Recently, Veeravagu et al. demonstrated in an orthotopic murine (GL26) glioblastoma model that in vivo changes in blood vessel permeability, as shown by DCE MRI, correlates with histologic quantification of vascular density and vessel caliber as well as with the molecular expression of angiogenic factors such as VEGF and angiopoietins (ANG-1 and ANG-2) [174].

DWI can also be used in cancer imaging to assess tumour cellularity and infiltration and to monitor response to therapy [175]. The apparent diffusion coefficient (ADC) of water has been found to increase in the early phase of anticancer therapies. Treatment-induced killing of tumour cells in a 9L brain glioma model, leading to a decrease of cell density in tumour tissue, results in an increase of the ADC that may be explained by destruction of tumour cells, widening of the extracellular space and a consequent increase in extracellular, relatively mobile water [176]. Moreover, the treatment-induced increase in ADC values occurs as early as 4-5 days after therapy onset and precedes volumetric tumour changes [169].

Although metabolic changes associated with intracranial tumour growth can be monitored with MRS [177] and can be used for brain tumour phenotyping [178] and to evaluate cell damage as early as 2-4 days after ganciclovir treatment in gene therapy of experimental gliomas [179], most information on the metabolic state of intracranial gliomas can be gained by PET imaging.

*3.3.2. PET*

Dependent on the radiotracer used, PET can reveal highly specific quantitative information on various processes, most of them related to the increased cell metabolic rate within gliomas [180]. The most commonly used radiotracers in brain tumour imaging are radiolabelled 2-$^{18}$F-fluoro-2-deoxy-D-glucose ([$^{18}$F]FDG), methyl-$^{11}$C-L-methionine ([$^{11}$C]MET), O-(2-$^{18}$F-fluoroethyl)-L-tyrosine ([$^{18}$F]FET) and 3′-deoxy-3′-$^{18}$F-fluoro-thymidine ([$^{18}$F]-FLT). These radiotracers are incorporated into proliferating gliomas depending on their tumour grade, as a reflection of the increased activity of membrane transporters for glucose ([$^{18}$F]FDG), amino acids ([$^{11}$C]MET and [$^{18}$F]FET) and nucleosides ([$^{18}$F]FLT) as well as the increased expression of cellular hexokinase ([$^{18}$F]FDG) and thymidine kinase ([$^{18}$F]FLT) and give information on energy metabolism ([$^{18}$F]FDG), protein synthesis ([$^{18}$F]FET) and DNA synthesis ([$^{18}$F]FLT) [181]. Furthermore, hypoxic tumour cells can be selectively labelled with radiolabelled derivatives of misonidazole (e.g. $^{18}$F-fluoromisonidazole, $^{18}$F-MISO) to evaluate tumour tissue oxygenation rate [182]. As tumour hypoxia is an independent predictor of outcome and is associated with chemo- and radioresistance, $^{18}$F-MISO PET imaging not only has the potential for defining the biological microenvironment of a tumour, but also can help in selecting and directing the appropriate treatment.

*3.3.3. Reporter-transgene imaging*

Many recent advances associated with imaging tumours in small animals have arisen from the application of reporter transgenes. Such transgene-based approaches have enabled the non-invasive measurement of a wide range of biological parameters with excellent tumour specificity [183]. The detection and measurement of luciferase activity (bioluminescence imaging), fluorescent protein excitation (fluorescence imaging) and herpes simplex type 1 thymidine kinase (HSV-1-*tk*) activity (PET) are among the most commonly applied transgene-based approaches for imaging in mice. Many different xenograft tumour cell lines constitutively express an optical imaging reporter gene. In small animal research, optical imaging is especially useful for rapid and accurate studies of tumour biology. It has been shown that there is a tight correlation between photon emission and gadolinium-enhanced MRI for intracranial tumour growth surveillance [184] [185] [186], and the growth dynamics of tumours or metastases can be accurately determined by quantification of the relative changes in light emission intensity over time. OI has also proved to be a particularly useful tool for measuring the efficacy of cancer therapeutics. For instance, bioluminescence imaging (BLI) has been used to monitor intracranial 9L gliosarcoma tumour cell kill following 1,3-bis(2-chloroethyl)-1-nitrosourea (BCNU) treatment [184] or to evaluate the response of intracranial glioblastoma xenografts to primary and salvage temozolomide therapy [187]. Also spatially restricted (tissue-specific) and temporally restricted (inducible) reporter transgene expression strategies have been employed extensively to image tumour dynamics in mice [188] [189] [190].

*3.3.4. Targeted ligand imaging*

The development of targeted imaging ligands has further enabled the non-invasive evaluation of diverse other aspects of in vivo tumour biology, such as tumour cell apoptosis, angiogenic blood vessels or expression of specific tumour antigens or signalling pathways with OI, PET

and to a lesser extent also MRI and have been used to evaluate the efficiency of therapies that target these specific molecular entities (see there).

### *3.4. Therapy*

Over the last years, notably within the field of tumour research, crucial improvements in the knowledge of genetic and molecular alterations at the basis of tumour development were made and allowed the development and use of a new generation of drugs that target specific molecular entities [191]. The development of such novel rationally targeted cancer therapies benefits significantly from efficient screening in biologically relevant systems as well as from the advances in targeted molecular imaging, not only in the assessment of drug targets (which could be used for patient selection) but also of early treatment response.

#### *3.4.1. Gene therapy*

Triggered by our experience in clinical gene therapy for patients with glioblastoma [192] [193], imaging-guided gene therapy paradigms for glioma models have been studied extensively by our group, where biological active target tissue for gene therapy vectors have been imaged by [$^{11}$C]MET- or [$^{18}$F]FLT-PET (**Figure 5A**), where transduction efficiency has been studied by OI or [$^{18}$F]FHBG-PET (**Figure 5A**), and where therapeutic efficiency of the gene therapy paradigm has been correlated to transduction efficiency (**Fig 5B, C**) and evaluated by [$^{11}$C]MET- or [$^{18}$F]FLT-PET (**Figure 6**) [194] [195]. Furthermore, we have shown that the quantification of transduced gene expression, which can be transriptionally regulated is possible by PET and OI **(Figure 7**) [189]. These imaging paradigms have important applications when designing protocols for transplantation of genes into diseased tissue in clinical application.

#### *3.4.2. Anti-angiogenic therapy*

A variety of genetic anomalies that trigger glioma-associated angiogenesis, such as overexpression of the growth factors VEGF, EGF, PDGF and their receptors or chronic activation of the hypoxia-inducible transcription factor-1 (HIF-1) have been identified and can be measured directly or indirectly by non-invasive imaging techniques and used as read-outs for targeted tumour treatment. Conventional imaging techniques like MRI and PET focus on the measurement of physiologic parameters, such as blood flow, blood volume, vascular perfusion, permeability and/or structure and represent the radiographic tools in current clinical trials of anti-angiogenic therapy [196]. During the last years, intense research focused on VEGF/VEGFR–targeted molecular imaging and a wide variety of targeting molecules (peptides, proteins, antibodies and nanoparticles) have been labelled with various imaging labels (such as radioisotopes, fluorescent dyes, and microbubbles) for PET, SPECT, optical imaging or contrast-enhanced ultrasound imaging of tumour angiogenesis [197, 198]. Hsu et al. [186] used multi-modality (BLI, MRI and PET) molecular imaging to determine the antiangiogenic and antitumour efficacies of a vasculature-targeting fusion toxin (VEGF(121)/rGel) composed of the VEGF-A isoform VEGF(121) linked with a G(4)S-tether to recombinant plant toxin gelonin (rGel) in an orthotopic glioblastoma mouse model. In this study, the level of target expression was monitored before therapy by [$^{64}$Cu]-1,4,7,10-tetraazacyclododedane-N,N',N'',N'''-tetraacetic acid (DOTA)-VEGF(121)/rGel PET, whereas [$^{18}$F]FLT scans were obtained before and after treatment to evaluate VEGF(121)/rGel therapeutic efficacy. In VEGF(121)/rGel-treated mice a significant decrease in [$^{18}$F]FLT uptake and peak BLI tumour signal intensities could be observed as compared to non-treated mice and these results were validated by histologic analysis.

Also expression of cell adhesion molecules, such as integrins, is significantly up-regulated during tumour growth and angiogenesis and αvβ3 expression has been correlated with tumour aggressiveness [199]. αvβ3 integrin expression can be measured by targeted radiolabelled

[200] [201], paramagnetic [202] and fluorescent [203] molecules (cyclic arginine-glycine-aspartic acid RGD peptides) and this method can be used to selectively target suicide gene therapy [204] or drug delivery [205]. Serganova et al. [206] developed a dual reporter gene cassette to monitor non-invasively the dynamics and spatial heterogeneity of HIF-1-specific transcriptional activity in tumours and showed that HIF-1-mediated activation of TKGFP (thymidine kinase green fluorescent protein; [207]) reporter gene expression in hypoxic tumour tissue can be non-invasively and repeatedly visualised in living mice using PET imaging with [$^{18}$F]-2'-fluoro-2'-deoxy-1β-D-arabionofuranosyl-5-ethyl-uracil (FEAU).
Nanoparticle technology has been shown to be a versatile tool for drug delivery. Nanoparticles can be used as vehicles for the delivery of imaging contrast agents and therapeutics in a targeted manner [208]. Reddy et al. [209] selectively targeted angiogenic endothelial cells within brain tumour vasculature with a nanoparticle formulation consisting of an encapsulated imaging agent (iron oxide or fluorescent) and a photosensitizer (Photofrin). The authors could show the feasibility of this method to detect significant MRI contrast enhancement in intracranial gliomas following i.v. nanoparticle administration and to specifically treat the gliomas after photodynamic therapy. The same technology can be used to target annexin conjugated nanoparticles composed of a fluorescent and paramagnetic label to apoptosis [210] [211].

*3.4.3. Apoptosis*

Aberrations of apoptotic signalling have been considered to be one of the hallmarks of cancer pathology [212] and therefore, the development of a quantitative technique to detect apoptosis non-invasively could provide immense advantages for evaluating therapeutic strategies in vivo (Lee, clin cancer res 2007). Modulating the apoptotic pathway by caspase inhibitors or activators represents special opportunities for therapeutic intervention and underline the need for non-invasive monitoring of early drug response at the molecular level. This can be achieved by direct imaging of caspase activity (e.g. caspase peptide substrates containing either a nuclear or a bioluminescence label [213] [214] [215] [216] or a near-infrared optical fluorochrome [217]) or by imaging the downstream effects on surface phosphatidylserine (PS) expression (e.g. radionuclide [218] [219], paramagnetic [220] or fluorochrome labelled Annexin V [221]). By means of such imaging paradigms the effect of apoptotic pathway regulating drugs can been identified [222] [214] [216]. This is particularly important, as there is already evidence, both from the laboratory and the clinic, that an early apoptotic response to therapy is a good prognostic indicator for treatment outcome [223]. It should be pointed out that E2F-1 mediated transcriptional regulation with E2F-1 being an important "decision marker" for uncontrolled proliferation or initiation of apoptosis can be non-invasively assessed by placing molecular imaging marker genes under transcriptional control of E2F-1 responsive promoter elements (**Figure 8**) [190].

*3.4.4. Cell therapy*

The use of neural stem cells (NSCs) for the treatment of brain tumours has attracted much interest in recent years [224]. The characteristics of NSCs that make them attractive vehicles for targeted delivery are their tropic behaviour towards neoplasms. Aboody and colleagues [225] first documented that modified exogenous NSCs injected into the contralateral hemispheres migrate over long distances to sites of gliomas in mice. Recently, several groups have reported promising results with extended survival [226] [227] or reduced tumour growth [225] [228] [229] [230] after neural stem cell-based gene therapy in animal models of high-grade gliomas. An intrinsic tumour-inhibition effect of neural stem cells has been observed after co-inoculation of NSCs with glioma cells [231] or grafting into established gliomas [226]. Also, due to the pluripotency of neural stem cells, a potential role of NSCs may be to

repair the damage caused by the brain tumours themselves and the neurological impairment that is frequently associated with traditional cancer treatment approaches [232].
Until recently, the in vivo study of particular populations of cells, such as NSCs, was mainly based on snapshot images from ex vivo histology. Thus, imaging techniques for *in vivo* longitudinal detection of the dynamics of these cells became desirable. Over the past years, the tumour targeting abilities of implanted neural stem and progenitor cells have been monitored non-invasively with various imaging modalities and most extensive information has been gained with optical imaging. Also cellular MR imaging techniques have been used increasingly and even PET imaging has been applied to detect stem cell migration and therapy in intracranial glioma models. By use of bioluminescence imaging systems, Shah and co-workers simultaneously monitored both the migration of NSCs toward gliomas and the efficacy of tumour necrosis factor-related apoptosis-inducing ligand (S-TRAIL) on the glioma burden in real time by dual enzyme substrate (Rluc/Fluc) imaging [230]. However, in general, BLI offers poor tissue penetration and poor spatial resolution. Miletic et al [233] together with our group used a multimodal imaging protocol combining multi-tracer PET and MRI to demonstrate that a subpopulation of bone marrow derived mesenchymal stem cells can be used as tumour-infiltrating therapeutic cells against malignant glioma. The stem cells genetically engineered to express HSV-1 thymidine kinase (TK) were injected into rat intracranial 9L gliomas. After transplantation, stem cell localization and distribution could be monitored non-invasively by means of the HSV-1 TK-specific PET radioligand 9-(4-fluoro-3-hydroxymethylbutyl)-guanine ([$^{18}$F]FHBG). In addition, the therapeutic effect of ganciclovir treatment could be monitored sequentially by MRI and [$^{11}$C]MET-PET and strongly correlated with histological analysis (**Figure 9**). Cellular imaging by MRI (cellular MRI) provides another non-invasive dynamic method for evaluating the seeding, migration and homing of magnetically labelled NSCs [234] [235], as well as an excellent soft tissue differentiation with a high spatial resolution. This led Zhang and co-workers [236] to successfully monitor neural progenitor cells labelled with superparamagnetic particles (SPIO) in a rat gliosarcoma model using *in vivo* MRI as they infiltrated the tumour mass or as they tracked down invading tumour cells. Also, migration and incorporation of magnetically labelled NSCs into the angiogenic vasculature of brain tumours has been studied [237] [238]. Brekke and colleagues [224] investigated the potential of cellular MR imaging to monitor *in vivo* the migration and infiltration of GRID-labelled murine NSCs (MHP36) from the seeding site to the tumour region in a rat glioma model using longitudinal multiparametric MRI. In addition, the authors were able to demonstrate the therapeutic potential of the mere injection of neural stem cells through an MRI-based measurement of tumour growth and development of vasogenic oedema. Fulci et al [239] used cellular MRI to non-invasively monitor innate immune response (MION-loaded macrophages) after glioma virotherapy in a syngeneic rat glioma model. Furthermore, the applied image protocol enabled the authors to image the increased efficiency of oncolytic virotherapy after preadministration of cyclophosphamide. This increased efficiency was credited to the immunosuppressive action of cyclophosphamide. However, it should be pointed out, that transplantation of mouse NPCs into the intact mouse brain can reveal signs of uncontrolled proliferation and migration even to distant areas (e.g. spinal cord) after various time points (**Figure 10**), indicating that molecular imaging should be used and implemented in the clinical applications of therapeutic stem cell technology to reveal signs of uncontrolled stem cell behaviour in vivo [240].

## 4. Conclusion

Continuous refinements in available mouse models together with improvements in small animal imaging techniques have recently led to a rapid progress in the variety of ways disease biology can be monitored non-invasively in living animals. Insights into the

pathophysiological processes related to disease initiation and progression resulted in the identification of new molecular targets or treatment strategies and functional imaging probes directed to disease-specific alterations have been developed and optimized. These advances increased our knowledge of *disease dynamics* and refined the design of effective therapeutic interventions in a true translational manner.

## 5. Future challenges

The ability of non-invasive imaging techniques to assess neurological disease states is beyond dispute.
In the near future, a careful validation of the applied imaging probes and imaging readouts need to be addressed. The establishment of effective molecular biomarkers or end-points capable of defining critical parameters, such as genetic signatures or metabolic and signalling states of specific disorders, will provide faster, more effective and less expensive ways to diagnose disorders, to evaluate drug efficacy and to define patient sub-groups more likely to have therapeutic benefit. Furthermore, the applied imaging protocols for disease diagnosis and therapy guidance need to be standardised in order to compare experimental results between research groups.
Ultimately, application of non-invasive imaging of neurological disorders will result in improved patient care and lead to patient-specific therapies with greater efficacies and fewer side effects.

## 6. Acknowledgments

Our work is supported in part by the Deutsche Forschungsgemeinschaft (DFG-Ja98/1-2), by the 6$^{th}$ FW EU grants EMIL (LSHC-CT-2004-503569), DiMI (LSHB-CT-2005-512146) and CliniGene NoE (LSHB-CT-2006-018933) and by the Bundesministerium für Bildung und Forschung (MoBiMed 01EZ0811).

## 7. Figure legends

***Figure 1:*** Schematic drawing of central dopamine processing at a synaptic terminal of a nigrostriatal dopamine (DA) neuron and its postsynaptic target, a striatal GABAergic projection neuron.
In the DA neuron, tyrosine is converted to DA in two steps: The first and rate-limiting step is the synthesis of L-3,4-dihydroxyphenylalanine (DOPA) by the enzyme tyrosine hydroxylase (TH). The second step is catalysed by aromatic amino acid decarboxylase (AADC). Newly synthesised cytoplasmic DA is then captured in specialised vesicles by the vesicular monoamine transporter-2 (VMAT2), stored and released into the synaptic cleft upon activation. On the post-synaptic side, DA binds to its specific receptors (D1 and D2 receptor families) to mediate its actions. DA is then either metabolised extraneuronally into homovanillic acid (HVA) by monoamine oxidase (MAO), or taken up by the presynaptic terminals by the dopamine transporter (DAT) to be re-vesicularised or metabolised into 3,4-dihydoxyphenylacetic acid (DOPAC) by catechol-O-methyl-transferase (COMT). Also the sites of action of four different PET ligands used for visualisation of the DA system are illustrated. First, radioactive fluorine substituted L-DOPA ([$^{18}$F]DOPA) uptake represents striatal uptake, AADC activity and presynaptic vesicular storage. A second way to label the presynaptic neurons is to use a specific ligands for the DAT (e.g. $^{11}$C-d-threomethylphenidate, [$^{11}$C]MP or [$^{123}$I]*N*-ω-fluoropropyl-2b-carbomethoxy-3b-(4-iodophenyl)nortropane, [$^{123}$I]FP-

CIT) or the VMAT2 (e.g $^{11}$C-dihydrotetrabenazine, [$^{11}$C]DTBZ). Finally the post-synaptic DA receptors can be labelled by using $^{11}$C-raclopride, $^{18}$F-spiperone or $^{123}$I-iodobenzamide ($^{123}$I-IBZM).

***Figure 2:*** Unaltered brain glucose metabolism in NIRKO mice.
Shown are representative high-resolution magnetic resonance images (upper) and matched [$^{18}$F]FDG microPET images (lower) through the brain of a representative control mouse (upper) and a representative NIRKO mouse (lower). ROIs were placed in a transaxial plane (arrow). Distinction between brain and hypermetabolic harderian glands (arrowhead) is made by coregistration with MRI (adapted from Schubert et al. PNAS 2004 with permission [97]).

***Figure 3:*** Altered cerebral glucose metabolism, neuronal integrity, and cholinergic function detected *in vivo* after noradrenergic depletion of APP23 mice.
**A.** Representative high-resolution magnetic resonance images (first row) and matched representative [$^{18}$F]FDG, [$^{11}$C]FMZ, and [$^{11}$C]MP4A microPET images (second–fourth rows, coronar is left; transaxial, middle; sagittal, right) through the brain of saline-treated (left panel) and dsp4-treated APP23 (right panel).
**B.** Quantification of [$^{18}$F]FDG, [$^{11}$C]FMZ, and [$^{11}$C]MP4A uptake in saline-treated wild-type (wt-con) and saline-treated APP23 (tg-con) mice at 13 months of age. No significant differences were detected.
**C.** Quantification of [$^{18}$F]FDG, [$^{11}$C]FMZ, and [$^{11}$C]MP4A uptake in saline-injected (tg-con) and dsp4-treated (tg-dsp4) APP23 transgenic mice at the same age revealed a decrease in all parameters after LC degeneration (mean+SEM; n=4 animals per group; Student's t test; *$p<0.05$) (adapted from Heneka et al. J Neurosc 2006 with permission [98]).

***Figure 4:*** Schematic representation of relevant signal transduction pathways and cell cycle control pathways known to be dysregulated and involved in glioma initiation and growth.
GF, growth factor; GFR, growth factor receptor; RTK, receptor tyrosine kinase; EGF, epidermal growth factor; VEGF, vascular endothelial growth factor; PDGF, platelet-derived growth factor and their respective receptors EGFR, VEGFR and PDGR; MAPK, mitogen-activated protein kinase; ERK, extracellular signal-regulated kinase; MEK, MAPK/ERK kinase; PLC, phospholipase C; PKC, protein kinase C; PI3K, phosphatidylinositol-3-kinase; PTEN, phosphatase and tensin homology deleted on chromosome 10; Akt, protein kinase B; mTOR, mammalian target of rapamycin; HIF-1, hypoxia-inducible factor-1; INK4a/ARF, Inhibitor of Kinase 4/Alternative Reading Frame tumour suppressor genes; CDK4, cyclin dependent kinase 4; MDM2, murine double minute 2 oncogene; p53, protein 53 transcription factor; Rb, retinoblastoma tumour suppressor protein; E2F1, transcription factor (activator) from E2F family of transcription factors

***Figure 5:*** Imaging-guided gene therapy paradigm.
**A.** Experimental protocol for identification of viable target tissue and assessment of vector-mediated gene expression *in vivo* in a mouse model with three subcutaneous gliomas. Row 1: localization of tumours is displayed by MRI. Row 2: the viable target tissue is displayed by [$^{18}$F]FDG-PET; note the signs of necrosis in the lateral portion of the left-sided tumour (arrow). Rows 3+4: following vector-application into the medial viable portion of the tumour (arrow) the tissue dose of vector-mediated gene expression is quantified by [$^{18}$F]FHBG-PET. Row 3 shows an image acquired early after tracer injection, which is used for coregistration; row 4 displays a late image with specific tracer accumulation in the tumour that is used for quantification (adapted from Jacobs, Rueger et al., with permission [194]).
**B.** Response to gene therapy correlates to therapeutic gene expression. The intensity of *cd*IRES*tk39gfp* expression, which is equivalent to transduction efficiency and tissue-dose of

vector mediated therapeutic gene expression, is measured by [$^{18}$F]FHBG-PET (in %ID/g), and the induced therapeutic effect is measured by [$^{18}$F]FLT-PET (R=0.73, p<0.01). Therapeutic effect ([$^{18}$F]FLT) was calculated as the difference between [$^{18}$F]FLT accumulation after and before therapy (adapted from Jacobs, Rueger et al., with permission [194]).
**C.** Relation between changes in volumetry and [$^{18}$F]FLT uptake. Changes in tumour volume and [$^{18}$F]FLT uptake were plotted for tumors grown in 11 nude mice. There is a strong correlation between volumetry and change in FLT uptake (R=0.83) for those tumours responding to therapy (complete responders) and a weaker correlation (R=0.57) for those tumors not responding to therapy (non responders). No correlation was found for those tumours where focal alterations of [$^{18}$F]FLT uptake occurred which did not lead to a reduction in overall tumour volume (partial responders; adapted from Jacobs, Rueger et al., with permission [194]).

***Figure 6:*** Multimodal imaging of response to vector-mediated gene therapy.
Shown are representative three-dimensional MR images (T1-weighted FLASH; echo time, 5 ms; repetition time, 70 ms; 60j pulse; resolution, 121 x 121 x 242 μm after administration of gadoliniumdiethylenetriaminepentaacetic acid; A1-A3, E1-E3 and G), [$^{18}$C]MET PET (B1-B3, D1-D3 and F) and [$^{18}$F]FHBG PET scans (C1-C3).
A1, B1, C1, D1, E1, F and G: 9LDsRed tumour-bearing rats that had received LCMV-tk-GFP injection with ganciclovi treatment. A2, B2, C2, D2 and E2: 9LDsRed tumour-bearing rats that had received LCMV-tk-GFP injection without ganciclovir treatment. A3, B3, C3, D3 and E3: 9LDsRed tumour-bearing rats that received only ganciclovir treatment.
Time points after tumour implantation: 6 d, MRI before ganciclovir treatment (A1-A3); 7 to 8 d, [$^{18}$C]MET PET before ganciclovir treatment (B1-B3); 9 d, [$^{18}$F]FHBG PET before ganciclovir treatment (C1-C3); 14 d, [$^{18}$C]MET PET during ganciclovir treatment (D1-D3); 15 d, MRI during ganciclovir treatment (E1-E3); 20 d, [$^{18}$C]MET PET after ganciclovir treatment (F); and 22 d, MRI after ganciclovir treatment (G) (adapted from Miletic et al., with permission [195]).

***Figure 7:*** In vivo bioluminescence imaging of exogenous gene regulation (induced luciferase (LUC) expression) and image validation by histology.
**A**. Temporal analysis of up- and down-regulation of LUC expression. HET-6C injection was performed intratumourally at day 0. Days where bioluminescent images were obtained are indicated at the upper right corner, days of doxycycline treatment at the top.
**B**. Quantitative analysis of luciferase signal (OFF-ON- OFF) in response to doxycycline.
**C**. Temporal analysis of up- and down-regulation of LUC expression in the intracranial glioma model (OFF-ON-OFF-ON). Indicated are the days of tumor growth.
**D**. Image validation by histology. BLI of a mouse bearing a subcutaneous glioma stably expressing LUC on its left shoulder after *in vivo* transduction with HET6C-luc in the tumour on the right shoulder. Representative histological sections taken from the *in vivo* transduced tumour showing co-localization of eGFP, expressed constitutively from the herpes viral immediate early 4/5 promoter, and RFP, expressed from the bi-directional regulated promoter (Unit for all colour scales as well as the histogram on temporal analysis was defined as photons/second/cm2/steradian (p/s/cm2/sr), scale bar overlay: 150 mm, exposure time: 0.5 s)(adapted from Winkeler et al. Plos One 2007 with permission [189]).

***Figure 8:*** Noninvasive imaging of E2F-1 mediated transcriptional regulation.
**A.** E2F-regulated cells and negative and positive control cells were implanted as a set of four tumours in the back of different groups of experimental mice. Mice were followed over time by bioluminescence imaging until tumours could be clearly visualised. Mice were then subjected to BCNU treatment (50%) or control treatment (50%), and repeat imaging was

performed 24 h later. An increased luciferase signal was observed only in mice bearing E2F-1-regulated cells and not in mice bearing negative and positive control cells. Color scale, luminescent signal intensity; blue, least intense signal; red, most intense signal.
**B.** mean of the total bioluminescent signals emitted from E2F-1–regulated tumours and negative and positive control tumours in response to BCNU administration. Columns, mean of three independent experiments with n = 6 animals per group; bars, SD. Significant differences are indicated by * ($P < 0.05$) and ** ($P < 0.05$) (modified from Monfared et al. with permission [190]).

***Figure 9:*** Multimodal imaging of cell-based glioma therapy.
Representative threedimensional MRI (T1-weighted FLASH, echo time = 5ms, repetition time = 70ms, 60° pulse, resolution 121 x 121 x 242µm, post-administration of gadopentetic acid (Gd-DTPA)), [$^{11}$C]MET PET and [$^{18}$F]FHBG PET scans. Time points after tumour implantation: (**a-c**) 6 days, MRI before ganciclovir (GC) treatment; (**d-f**) 7-8 days, [$^{11}$C]MET PET before GC treatment; (**g-i**) 12 days, [$^{18}$F]FHBG PET during GC treatment; (**j-l**) 13 days, MRI during GC treatment; (**m-o**) 14 days, [$^{11}$C]MET PET during GC treatment; (**p**) 21 days, MRI after GC treatment; (**q**) 22 days, [$^{11}$C]MET PET after GC treatment. The three different groups were treated as following: (**a, d, g, j, m, p, q**) bone-marrow derived tumour infiltrating cells expressing thymidine kinase and green fluorescent protein (BM-TIC-tk-GFP) injection with GC treatment; (**b, e, h, k, n**) BM-TIC-tk-GFP injection without GC treatment; (**c, f, i, l, o**) 9LDsRed gliomas only with GC treatment (adapted from Miletic et al. Mol Ther 2007 with permission [233]).

***Figure 10:*** Bioluminescence imaging of aberrant stem cell migration.
Murine neural progenitor cells genetically engineered to express luciferase, HSV-1-*tk* and GFP (C17.2-LITG cells) were injected into the left striatum of a non-glioma-bearing mouse and their behaviour over time was monitored with optical imaging. NPC migration in the direction of the cerebellar hemispheres (red arrow) could be demonstrated 13 days after injection (red arrow); at 3 weeks, NPCs also localized at the level of the thoracolumbar spine (green arrow) (adapted from Waerzeggers et al. 2008 with permission [240]).

## 8. Literature

1. Strome EM, Doudet DJ. Animal models of neurodegenerative disease: insights from in vivo imaging studies. Mol Imaging Biol 2007;9(4):186-95.
2. Bernheimer H, Birkmayer W, Hornykiewicz O, Jellinger K, Seitelberger F. Brain dopamine and the syndromes of Parkinson and Huntington. Clinical, morphological and neurochemical correlations. J Neurol Sci 1973;20(4):415-55.
3. Fearnley JM, Lees AJ. Ageing and Parkinson's disease: substantia nigra regional selectivity. Brain 1991;114 ( Pt 5):2283-301.
4. de la Fuente-Fernandez R, Calne DB. Evidence for environmental causation of Parkinson's disease. Parkinsonism Relat Disord 2002;8(4):235-41.
5. Tolosa E, Wenning G, Poewe W. The diagnosis of Parkinson's disease. Lancet Neurol 2006;5(1):75-86.
6. Bonifati V, Oostra BA, Heutink P. Unraveling the pathogenesis of Parkinson's disease--the contribution of monogenic forms. Cell Mol Life Sci 2004;61(14):1729-50.
7. Melrose HL, Lincoln SJ, Tyndall GM, Farrer MJ. Parkinson's disease: a rethink of rodent models. Exp Brain Res 2006;173(2):196-204.
8. Bove J, Prou D, Perier C, Przedborski S. Toxin-induced models of Parkinson's disease. NeuroRx 2005;2(3):484-94.

9. Fleming SM, Fernagut PO, Chesselet MF. Genetic mouse models of parkinsonism: strengths and limitations. NeuroRx 2005;2(3):495-503.
10. Cohen G. Oxy-radical toxicity in catecholamine neurons. Neurotoxicology 1984;5(1):77-82.
11. Liou HH, Tsai MC, Chen CJ, Jeng JS, Chang YC, Chen SY, et al. Environmental risk factors and Parkinson's disease: a case-control study in Taiwan. Neurology 1997;48(6):1583-8.
12. Manning-Bog AB, McCormack AL, Li J, Uversky VN, Fink AL, Di Monte DA. The herbicide paraquat causes up-regulation and aggregation of alpha-synuclein in mice: paraquat and alpha-synuclein. J Biol Chem 2002;277(3):1641-4.
13. Sherer TB, Kim JH, Betarbet R, Greenamyre JT. Subcutaneous rotenone exposure causes highly selective dopaminergic degeneration and alpha-synuclein aggregation. Exp Neurol 2003;179(1):9-16.
14. McNaught KS, Perl DP, Brownell AL, Olanow CW. Systemic exposure to proteasome inhibitors causes a progressive model of Parkinson's disease. Ann Neurol 2004;56(1):149-62.
15. Kahle PJ. alpha-Synucleinopathy models and human neuropathology: similarities and differences. Acta Neuropathol 2008;115(1):87-95.
16. Harvey BK, Wang Y, Hoffer BJ. Transgenic rodent models of Parkinson's disease. Acta Neurochir Suppl 2008;101:89-92.
17. Nagano-Saito A, Washimi Y, Arahata Y, Kachi T, Lerch JP, Evans AC, et al. Cerebral atrophy and its relation to cognitive impairment in Parkinson disease. Neurology 2005;64(2):224-9.
18. Burton EJ, McKeith IG, Burn DJ, Williams ED, O'Brien JT. Cerebral atrophy in Parkinson's disease with and without dementia: a comparison with Alzheimer's disease, dementia with Lewy bodies and controls. Brain 2004;127(Pt 4):791-800.
19. Dagher A, Nagano-Saito A. Functional and anatomical magnetic resonance imaging in Parkinson's disease. Mol Imaging Biol 2007;9(4):234-42.
20. Clarke CE, Lowry M. Systematic review of proton magnetic resonance spectroscopy of the striatum in parkinsonian syndromes. Eur J Neurol 2001;8(6):573-7.
21. Ravina B, Eidelberg D, Ahlskog JE, Albin RL, Brooks DJ, Carbon M, et al. The role of radiotracer imaging in Parkinson disease. Neurology 2005;64(2):208-15.
22. Au WL, Adams JR, Troiano AR, Stoessl AJ. Parkinson's disease: in vivo assessment of disease progression using positron emission tomography. Brain Res Mol Brain Res 2005;134(1):24-33.
23. Doudet DJ, Chan GL, Holden JE, McGeer EG, Aigner TA, Wyatt RJ, et al. 6-[18F]Fluoro-L-DOPA PET studies of the turnover of dopamine in MPTP-induced parkinsonism in monkeys. Synapse 1998;29(3):225-32.
24. Melega WP, Raleigh MJ, Stout DB, DeSalles AA, Cherry SR, Blurton-Jones M, et al. Longitudinal behavioral and 6-[18F]fluoro-L-DOPA-PET assessment in MPTP-hemiparkinsonian monkeys. Exp Neurol 1996;141(2):318-29.
25. Schneider JS, Lidsky TI, Hawks T, Mazziotta JC, Hoffman JM. Differential recovery of volitional motor function, lateralized cognitive function, dopamine agonist-induced rotation and dopaminergic parameters in monkeys made hemi-parkinsonian by intracarotid MPTP infusion. Brain Res 1995;672(1-2):112-7.
26. Hantraye P, Brownell AL, Elmaleh D, Spealman RD, Wullner U, Brownell GL, et al. Dopamine fiber detection by [11C]-CFT and PET in a primate model of parkinsonism. Neuroreport 1992;3(3):265-8.
27. Wullner U, Pakzaban P, Brownell AL, Hantraye P, Burns L, Shoup T, et al. Dopamine terminal loss and onset of motor symptoms in MPTP-treated monkeys: a positron emission tomography study with 11C-CFT. Exp Neurol 1994;126(2):305-9.

28. Brownell AL, Jenkins BG, Isacson O. Dopamine imaging markers and predictive mathematical models for progressive degeneration in Parkinson's disease. Biomed Pharmacother 1999;53(3):131-40.
29. Brownell AL, Canales K, Chen YI, Jenkins BG, Owen C, Livni E, et al. Mapping of brain function after MPTP-induced neurotoxicity in a primate Parkinson's disease model. Neuroimage 2003;20(2):1064-75.
30. Doudet DJ, Jivan S, Ruth TJ, Holden JE. Density and affinity of the dopamine D2 receptors in aged symptomatic and asymptomatic MPTP-treated monkeys: PET studies with [11C]raclopride. Synapse 2002;44(3):198-202.
31. Hantraye P, Loc'h C, Tacke U, Riche D, Stulzaft O, Doudet D, et al. "In vivo" visualization by positron emission tomography of the progressive striatal dopamine receptor damage occurring in MPTP-intoxicated non-human primates. Life Sci 1986;39(15):1375-82.
32. Sharma SK, Ebadi M. Distribution kinetics of 18F-DOPA in weaver mutant mice. Brain Res Mol Brain Res 2005;139(1):23-30.
33. Sharma SK, El Refaey H, Ebadi M. Complex-1 activity and 18F-DOPA uptake in genetically engineered mouse model of Parkinson's disease and the neuroprotective role of coenzyme Q10. Brain Res Bull 2006;70(1):22-32.
34. Hume SP, Lammertsma AA, Myers R, Rajeswaran S, Bloomfield PM, Ashworth S, et al. The potential of high-resolution positron emission tomography to monitor striatal dopaminergic function in rat models of disease. J Neurosci Methods 1996;67(2):103-12.
35. Doudet DJ, Rosa-Neto P, Munk OL, Ruth TJ, Jivan S, Cumming P. Effect of age on markers for monoaminergic neurons of normal and MPTP-lesioned rhesus monkeys: a multi-tracer PET study. Neuroimage 2006;30(1):26-35.
36. Lee CS, Samii A, Sossi V, Ruth TJ, Schulzer M, Holden JE, et al. In vivo positron emission tomographic evidence for compensatory changes in presynaptic dopaminergic nerve terminals in Parkinson's disease. Ann Neurol 2000;47(4):493-503.
37. Yee RE, Irwin I, Milonas C, Stout DB, Huang SC, Shoghi-Jadid K, et al. Novel observations with FDOPA-PET imaging after early nigrostriatal damage. Mov Disord 2001;16(5):838-48.
38. Cohen RM, Carson RE, Aigner TG, Doudet DJ. Opiate receptor avidity is reduced in non-motor impaired MPTP-lesioned rhesus monkeys. Brain Res 1998;806(2):292-6.
39. Doudet DJ, Miyake H, Finn RT, McLellan CA, Aigner TG, Wan RQ, et al. 6-18F-L-dopa imaging of the dopamine neostriatal system in normal and clinically normal MPTP-treated rhesus monkeys. Exp Brain Res 1989;78(1):69-80.
40. Guttman M, Yong VW, Kim SU, Calne DB, Martin WR, Adam MJ, et al. Asymptomatic striatal dopamine depletion: PET scans in unilateral MPTP monkeys. Synapse 1988;2(5):469-73.
41. Strome EM, Cepeda IL, Sossi V, Doudet DJ. Evaluation of the integrity of the dopamine system in a rodent model of Parkinson's disease: small animal positron emission tomography compared to behavioral assessment and autoradiography. Mol Imaging Biol 2006;8(5):292-9.
42. Hume SP, Opacka-Juffry J, Myers R, Ahier RG, Ashworth S, Brooks DJ, et al. Effect of L-dopa and 6-hydroxydopamine lesioning on [11C]raclopride binding in rat striatum, quantified using PET. Synapse 1995;21(1):45-53.
43. Nikolaus S, Larisch R, Beu M, Forutan F, Vosberg H, Muller-Gartner HW. Bilateral increase in striatal dopamine D2 receptor density in the 6-hydroxydopamine-lesioned rat: a serial in vivo investigation with small animal PET. Eur J Nucl Med Mol Imaging 2003;30(3):390-5.
44. Cicchetti F, Brownell AL, Williams K, Chen YI, Livni E, Isacson O. Neuroinflammation of the nigrostriatal pathway during progressive 6-OHDA dopamine

degeneration in rats monitored by immunohistochemistry and PET imaging. Eur J Neurosci 2002;15(6):991-8.
45. Sanchez-Pernaute R, Ferree A, Cooper O, Yu M, Brownell AL, Isacson O. Selective COX-2 inhibition prevents progressive dopamine neuron degeneration in a rat model of Parkinson's disease. J Neuroinflammation 2004;1(1):6.
46. Chen YC, Galpern WR, Brownell AL, Matthews RT, Bogdanov M, Isacson O, et al. Detection of dopaminergic neurotransmitter activity using pharmacologic MRI: correlation with PET, microdialysis, and behavioral data. Magn Reson Med 1997;38(3):389-98.
47. Nguyen TV, Brownell AL, Iris Chen YC, Livni E, Coyle JT, Rosen BR, et al. Detection of the effects of dopamine receptor supersensitivity using pharmacological MRI and correlations with PET. Synapse 2000;36(1):57-65.
48. Lauwers E, Beque D, Van Laere K, Nuyts J, Bormans G, Mortelmans L, et al. Non-invasive imaging of neuropathology in a rat model of alpha-synuclein overexpression. Neurobiol Aging 2007;28(2):248-57.
49. Obeso JA, Olanow CW, Nutt JG. Levodopa motor complications in Parkinson's disease. Trends Neurosci 2000;23(10 Suppl):S2-7.
50. Whone AL, Watts RL, Stoessl AJ, Davis M, Reske S, Nahmias C, et al. Slower progression of Parkinson's disease with ropinirole versus levodopa: The REAL-PET study. Ann Neurol 2003;54(1):93-101.
51. Dopamine transporter brain imaging to assess the effects of pramipexole vs levodopa on Parkinson disease progression. JAMA 2002;287(13):1653-61.
52. Fahn S, Oakes D, Shoulson I, Kieburtz K, Rudolph A, Lang A, et al. Levodopa and the progression of Parkinson's disease. N Engl J Med 2004;351(24):2498-508.
53. Jacobs AH, Winkler A, Castro MG, Lowenstein P. Human gene therapy and imaging in neurological diseases. Eur J Nucl Med Mol Imaging 2005;32 Suppl 2:S358-83.
54. Leriche L, Bjorklund T, Breysse N, Besret L, Gregoire MC, Carlsson T, et al. Positron emission tomography imaging demonstrates correlation between behavioral recovery and correction of dopamine neurotransmission after gene therapy. J Neurosci 2009;29(5):1544-53.
55. Lin LF, Doherty DH, Lile JD, Bektesh S, Collins F. GDNF: a glial cell line-derived neurotrophic factor for midbrain dopaminergic neurons. Science 1993;260(5111):1130-2.
56. Hyman C, Hofer M, Barde YA, Juhasz M, Yancopoulos GD, Squinto SP, et al. BDNF is a neurotrophic factor for dopaminergic neurons of the substantia nigra. Nature 1991;350(6315):230-2.
57. Bjorklund A, Kirik D, Rosenblad C, Georgievska B, Lundberg C, Mandel RJ. Towards a neuroprotective gene therapy for Parkinson's disease: use of adenovirus, AAV and lentivirus vectors for gene transfer of GDNF to the nigrostriatal system in the rat Parkinson model. Brain Res 2000;886(1-2):82-98.
58. Kirik D, Rosenblad C, Bjorklund A, Mandel RJ. Long-term rAAV-mediated gene transfer of GDNF in the rat Parkinson's model: intrastriatal but not intranigral transduction promotes functional regeneration in the lesioned nigrostriatal system. J Neurosci 2000;20(12):4686-700.
59. Kordower JH, Emborg ME, Bloch J, Ma SY, Chu Y, Leventhal L, et al. Neurodegeneration prevented by lentiviral vector delivery of GDNF in primate models of Parkinson's disease. Science 2000;290(5492):767-73.
60. Gash DM, Zhang Z, Ovadia A, Cass WA, Yi A, Simmerman L, et al. Functional recovery in parkinsonian monkeys treated with GDNF. Nature 1996;380(6571):252-5.
61. Tomac A, Lindqvist E, Lin LF, Ogren SO, Young D, Hoffer BJ, et al. Protection and repair of the nigrostriatal dopaminergic system by GDNF in vivo. Nature 1995;373(6512):335-9.

62. Kishima H, Poyot T, Bloch J, Dauguet J, Conde F, Dolle F, et al. Encapsulated GDNF-producing C2C12 cells for Parkinson's disease: a pre-clinical study in chronic MPTP-treated baboons. Neurobiol Dis 2004;16(2):428-39.
63. Sullivan AM, Opacka-Juffry J, Blunt SB. Long-term protection of the rat nigrostriatal dopaminergic system by glial cell line-derived neurotrophic factor against 6-hydroxydopamine in vivo. Eur J Neurosci 1998;10(1):57-63.
64. Opacka-Juffry J, Ashworth S, Hume SP, Martin D, Brooks DJ, Blunt SB. GDNF protects against 6-OHDA nigrostriatal lesion: in vivo study with microdialysis and PET. Neuroreport 1995;7(1):348-52.
65. Storch A, Hofer A, Kruger R, Schulz JB, Winkler J, Gerlach M. New developments in diagnosis and treatment of Parkinson's disease--from basic science to clinical applications. J Neurol 2004;251 Suppl 6:VI/33-8.
66. Bjorklund LM, Sanchez-Pernaute R, Chung S, Andersson T, Chen IY, McNaught KS, et al. Embryonic stem cells develop into functional dopaminergic neurons after transplantation in a Parkinson rat model. Proc Natl Acad Sci U S A 2002;99(4):2344-9.
67. Kim JH, Auerbach JM, Rodriguez-Gomez JA, Velasco I, Gavin D, Lumelsky N, et al. Dopamine neurons derived from embryonic stem cells function in an animal model of Parkinson's disease. Nature 2002;418(6893):50-6.
68. Lee SH, Lumelsky N, Studer L, Auerbach JM, McKay RD. Efficient generation of midbrain and hindbrain neurons from mouse embryonic stem cells. Nat Biotechnol 2000;18(6):675-9.
69. Carvey PM, Ling ZD, Sortwell CE, Pitzer MR, McGuire SO, Storch A, et al. A clonal line of mesencephalic progenitor cells converted to dopamine neurons by hematopoietic cytokines: a source of cells for transplantation in Parkinson's disease. Exp Neurol 2001;171(1):98-108.
70. Schwarz SC, Wittlinger J, Schober R, Storch A, Schwarz J. Transplantation of human neural precursor cells in the 6-OHDA lesioned rats: effect of immunosuppression with cyclosporine A. Parkinsonism Relat Disord 2006;12(5):302-8.
71. Bakay RA, Raiser CD, Stover NP, Subramanian T, Cornfeldt ML, Schweikert AW, et al. Implantation of Spheramine in advanced Parkinson's disease (PD). Front Biosci 2004;9:592-602.
72. Freed CR, Greene PE, Breeze RE, Tsai WY, DuMouchel W, Kao R, et al. Transplantation of embryonic dopamine neurons for severe Parkinson's disease. N Engl J Med 2001;344(10):710-9.
73. Olanow CW, Goetz CG, Kordower JH, Stoessl AJ, Sossi V, Brin MF, et al. A double-blind controlled trial of bilateral fetal nigral transplantation in Parkinson's disease. Ann Neurol 2003;54(3):403-14.
74. Walczak P, Bulte JW. The role of noninvasive cellular imaging in developing cell-based therapies for neurodegenerative disorders. Neurodegener Dis 2007;4(4):306-13.
75. Brooks DJ. Positron emission tomography imaging of transplant function. NeuroRx 2004;1(4):482-91.
76. Brownell AL, Livni E, Galpern W, Isacson O. In vivo PET imaging in rat of dopamine terminals reveals functional neural transplants. Ann Neurol 1998;43(3):387-90.
77. Chen YI, Brownell AL, Galpern W, Isacson O, Bogdanov M, Beal MF, et al. Detection of dopaminergic cell loss and neural transplantation using pharmacological MRI, PET and behavioral assessment. Neuroreport 1999;10(14):2881-6.
78. Hardy J. The shorter amyloid cascade hypothesis. Neurobiol Aging 1999;20(1):85; discussion 87.
79. Selkoe DJ. Alzheimer's disease results from the cerebral accumulation and cytotoxicity of amyloid beta-protein. J Alzheimers Dis 2001;3(1):75-80.

80. Laws SM, Hone E, Gandy S, Martins RN. Expanding the association between the APOE gene and the risk of Alzheimer's disease: possible roles for APOE promoter polymorphisms and alterations in APOE transcription. J Neurochem 2003;84(6):1215-36.
81. Hardy J, Selkoe DJ. The amyloid hypothesis of Alzheimer's disease: progress and problems on the road to therapeutics. Science 2002;297(5580):353-6.
82. Nordberg A. Amyloid imaging in Alzheimer's disease. Curr Opin Neurol 2007;20(4):398-402.
83. Spillantini MG, Murrell JR, Goedert M, Farlow MR, Klug A, Ghetti B. Mutation in the tau gene in familial multiple system tauopathy with presenile dementia. Proc Natl Acad Sci U S A 1998;95(13):7737-41.
84. Poorkaj P, Bird TD, Wijsman E, Nemens E, Garruto RM, Anderson L, et al. Tau is a candidate gene for chromosome 17 frontotemporal dementia. Ann Neurol 1998;43(6):815-25.
85. Meguro K, Blaizot X, Kondoh Y, Le Mestric C, Baron JC, Chavoix C. Neocortical and hippocampal glucose hypometabolism following neurotoxic lesions of the entorhinal and perirhinal cortices in the non-human primate as shown by PET. Implications for Alzheimer's disease. Brain 1999;122 ( Pt 8):1519-31.
86. Millien I, Blaizot X, Giffard C, Mezenge F, Insausti R, Baron JC, et al. Brain glucose hypometabolism after perirhinal lesions in baboons: implications for Alzheimer disease and aging. J Cereb Blood Flow Metab 2002;22(10):1248-61.
87. Bhagat YA, Obenaus A, Richardson JS, Kendall EJ. Evolution of beta-amyloid induced neuropathology: magnetic resonance imaging and anatomical comparisons in the rodent hippocampus. MAGMA 2002;14(3):223-32.
88. Xiao-Chuan W, Zheng-Hui H, Zheng-Yu F, Yue F, Yun-Huang Y, Qun W, et al. Correlation of Alzheimer-like tau hyperphosphorylation and fMRI bold intensity. Curr Alzheimer Res 2004;1(2):143-8.
89. Higgins GA, Jacobsen H. Transgenic mouse models of Alzheimer's disease: phenotype and application. Behav Pharmacol 2003;14(5-6):419-38.
90. Gotz J, Ittner LM. Animal models of Alzheimer's disease and frontotemporal dementia. Nat Rev Neurosci 2008;9(7):532-44.
91. Klunk WE, Engler H, Nordberg A, Wang Y, Blomqvist G, Holt DP, et al. Imaging brain amyloid in Alzheimer's disease with Pittsburgh Compound-B. Ann Neurol 2004;55(3):306-19.
92. Toyama H, Ye D, Ichise M, Liow JS, Cai L, Jacobowitz D, et al. PET imaging of brain with the beta-amyloid probe, [11C]6-OH-BTA-1, in a transgenic mouse model of Alzheimer's disease. Eur J Nucl Med Mol Imaging 2005;32(5):593-600.
93. Klunk WE, Lopresti BJ, Ikonomovic MD, Lefterov IM, Koldamova RP, Abrahamson EE, et al. Binding of the positron emission tomography tracer Pittsburgh compound-B reflects the amount of amyloid-beta in Alzheimer's disease brain but not in transgenic mouse brain. J Neurosci 2005;25(46):10598-606.
94. Bacskai BJ, Hickey GA, Skoch J, Kajdasz ST, Wang Y, Huang GF, et al. Four-dimensional multiphoton imaging of brain entry, amyloid binding, and clearance of an amyloid-beta ligand in transgenic mice. Proc Natl Acad Sci U S A 2003;100(21):12462-7.
95. Maeda J, Ji B, Irie T, Tomiyama T, Maruyama M, Okauchi T, et al. Longitudinal, quantitative assessment of amyloid, neuroinflammation, and anti-amyloid treatment in a living mouse model of Alzheimer's disease enabled by positron emission tomography. J Neurosci 2007;27(41):10957-68.
96. Valla J, Chen K, Berndt JD, Gonzalez-Lima F, Cherry SR, Games D, et al. Effects of image resolution on autoradiographic measurements of posterior cingulate activity in PDAPP mice: implications for functional brain imaging studies of transgenic mouse models of Alzheimer's Disease. Neuroimage 2002;16(1):1-6.

97. Schubert M, Gautam D, Surjo D, Ueki K, Baudler S, Schubert D, et al. Role for neuronal insulin resistance in neurodegenerative diseases. Proc Natl Acad Sci U S A 2004;101(9):3100-5.
98. Heneka MT, Ramanathan M, Jacobs AH, Dumitrescu-Ozimek L, Bilkei-Gorzo A, Debeir T, et al. Locus ceruleus degeneration promotes Alzheimer pathogenesis in amyloid precursor protein 23 transgenic mice. J Neurosci 2006;26(5):1343-54.
99. Rudin M, Mueggler T, Allegrini PR, Baumann D, Rausch M. Characterization of CNS disorders and evaluation of therapy using structural and functional MRI. Anal Bioanal Chem 2003;377(6):973-81.
100. Sykova E, Vorisek I, Antonova T, Mazel T, Meyer-Luehmann M, Jucker M, et al. Changes in extracellular space size and geometry in APP23 transgenic mice: a model of Alzheimer's disease. Proc Natl Acad Sci U S A 2005;102(2):479-84.
101. Sun SW, Song SK, Harms MP, Lin SJ, Holtzman DM, Merchant KM, et al. Detection of age-dependent brain injury in a mouse model of brain amyloidosis associated with Alzheimer's disease using magnetic resonance diffusion tensor imaging. Exp Neurol 2005;191(1):77-85.
102. Jack CR, Jr., Garwood M, Wengenack TM, Borowski B, Curran GL, Lin J, et al. In vivo visualization of Alzheimer's amyloid plaques by magnetic resonance imaging in transgenic mice without a contrast agent. Magn Reson Med 2004;52(6):1263-71.
103. Lee SP, Falangola MF, Nixon RA, Duff K, Helpern JA. Visualization of beta-amyloid plaques in a transgenic mouse model of Alzheimer's disease using MR microscopy without contrast reagents. Magn Reson Med 2004;52(3):538-44.
104. Vanhoutte G, Dewachter I, Borghgraef P, Van Leuven F, Van der Linden A. Noninvasive in vivo MRI detection of neuritic plaques associated with iron in APP[V717I] transgenic mice, a model for Alzheimer's disease. Magn Reson Med 2005;53(3):607-13.
105. Jack CR, Jr., Wengenack TM, Reyes DA, Garwood M, Curran GL, Borowski BJ, et al. In vivo magnetic resonance microimaging of individual amyloid plaques in Alzheimer's transgenic mice. J Neurosci 2005;25(43):10041-8.
106. Dhenain M, Privat N, Duyckaerts C, Jacobs RE. Senile plaques do not induce susceptibility effects in T2*-weighted MR microscopic images. NMR Biomed 2002;15(3):197-203.
107. Anderson SA, Frank JA. MRI of mouse models of neurological disorders. NMR Biomed 2007;20(3):200-15.
108. Poduslo JF, Wengenack TM, Curran GL, Wisniewski T, Sigurdsson EM, Macura SI, et al. Molecular targeting of Alzheimer's amyloid plaques for contrast-enhanced magnetic resonance imaging. Neurobiol Dis 2002;11(2):315-29.
109. Wadghiri YZ, Sigurdsson EM, Sadowski M, Elliott JI, Li Y, Scholtzova H, et al. Detection of Alzheimer's amyloid in transgenic mice using magnetic resonance microimaging. Magn Reson Med 2003;50(2):293-302.
110. Wengenack TM, Jack CR, Jr., Garwood M, Poduslo JF. MR microimaging of amyloid plaques in Alzheimer's disease transgenic mice. Eur J Nucl Med Mol Imaging 2008;35 Suppl 1:S82-8.
111. Higuchi M, Iwata N, Matsuba Y, Sato K, Sasamoto K, Saido TC. 19F and 1H MRI detection of amyloid beta plaques in vivo. Nat Neurosci 2005;8(4):527-33.
112. Miller BL, Moats RA, Shonk T, Ernst T, Woolley S, Ross BD. Alzheimer disease: depiction of increased cerebral myo-inositol with proton MR spectroscopy. Radiology 1993;187(2):433-7.
113. von Kienlin M, Kunnecke B, Metzger F, Steiner G, Richards JG, Ozmen L, et al. Altered metabolic profile in the frontal cortex of PS2APP transgenic mice, monitored throughout their life span. Neurobiol Dis 2005;18(1):32-9.

114. Mueggler T, Sturchler-Pierrat C, Baumann D, Rausch M, Staufenbiel M, Rudin M. Compromised hemodynamic response in amyloid precursor protein transgenic mice. J Neurosci 2002;22(16):7218-24.
115. Mueggler T, Baumann D, Rausch M, Staufenbiel M, Rudin M. Age-dependent impairment of somatosensory response in the amyloid precursor protein 23 transgenic mouse model of Alzheimer's disease. J Neurosci 2003;23(23):8231-6.
116. Farlow MR, Cummings JL. Effective pharmacologic management of Alzheimer's disease. Am J Med 2007;120(5):388-97.
117. Lichtlen P, Mohajeri MH. Antibody-based approaches in Alzheimer's research: safety, pharmacokinetics, metabolism, and analytical tools. J Neurochem 2008;104(4):859-74.
118. Schenk D, Barbour R, Dunn W, Gordon G, Grajeda H, Guido T, et al. Immunization with amyloid-beta attenuates Alzheimer-disease-like pathology in the PDAPP mouse. Nature 1999;400(6740):173-7.
119. Janus C, Pearson J, McLaurin J, Mathews PM, Jiang Y, Schmidt SD, et al. A beta peptide immunization reduces behavioural impairment and plaques in a model of Alzheimer's disease. Nature 2000;408(6815):979-82.
120. Sigurdsson EM, Knudsen E, Asuni A, Fitzer-Attas C, Sage D, Quartermain D, et al. An attenuated immune response is sufficient to enhance cognition in an Alzheimer's disease mouse model immunized with amyloid-beta derivatives. J Neurosci 2004;24(28):6277-82.
121. Bard F, Cannon C, Barbour R, Burke RL, Games D, Grajeda H, et al. Peripherally administered antibodies against amyloid beta-peptide enter the central nervous system and reduce pathology in a mouse model of Alzheimer disease. Nat Med 2000;6(8):916-9.
122. DeMattos RB, Bales KR, Cummins DJ, Dodart JC, Paul SM, Holtzman DM. Peripheral anti-A beta antibody alters CNS and plasma A beta clearance and decreases brain A beta burden in a mouse model of Alzheimer's disease. Proc Natl Acad Sci U S A 2001;98(15):8850-5.
123. Wisniewski T, Frangione B. Immunological and anti-chaperone therapeutic approaches for Alzheimer disease. Brain Pathol 2005;15(1):72-7.
124. Nicoll JA, Wilkinson D, Holmes C, Steart P, Markham H, Weller RO. Neuropathology of human Alzheimer disease after immunization with amyloid-beta peptide: a case report. Nat Med 2003;9(4):448-52.
125. Permanne B, Adessi C, Saborio GP, Fraga S, Frossard MJ, Van Dorpe J, et al. Reduction of amyloid load and cerebral damage in a transgenic mouse model of Alzheimer's disease by treatment with a beta-sheet breaker peptide. FASEB J 2002;16(8):860-2.
126. Sadowski MJ, Pankiewicz J, Scholtzova H, Mehta PD, Prelli F, Quartermain D, et al. Blocking the apolipoprotein E/amyloid-beta interaction as a potential therapeutic approach for Alzheimer's disease. Proc Natl Acad Sci U S A 2006;103(49):18787-92.
127. Tuszynski MH. Nerve growth factor gene therapy in Alzheimer disease. Alzheimer Dis Assoc Disord 2007;21(2):179-89.
128. Tuszynski MH. Nerve growth factor gene delivery: animal models to clinical trials. Dev Neurobiol 2007;67(9):1204-15.
129. Kaplan DR, Miller FD. Neurotrophin signal transduction in the nervous system. Curr Opin Neurobiol 2000;10(3):381-91.
130. Aicardi G, Argilli E, Cappello S, Santi S, Riccio M, Thoenen H, et al. Induction of long-term potentiation and depression is reflected by corresponding changes in secretion of endogenous brain-derived neurotrophic factor. Proc Natl Acad Sci U S A 2004;101(44):15788-92.
131. Williams LR, Varon S, Peterson GM, Wictorin K, Fischer W, Bjorklund A, et al. Continuous infusion of nerve growth factor prevents basal forebrain neuronal death after fimbria fornix transection. Proc Natl Acad Sci U S A 1986;83(23):9231-5.

132. Tuszynski MH, U HS, Amaral DG, Gage FH. Nerve growth factor infusion in the primate brain reduces lesion-induced cholinergic neuronal degeneration. J Neurosci 1990;10(11):3604-14.
133. Williams LR. Hypophagia is induced by intracerebroventricular administration of nerve growth factor. Exp Neurol 1991;113(1):31-7.
134. Isaacson LG, Saffran BN, Crutcher KA. Intracerebral NGF infusion induces hyperinnervation of cerebral blood vessels. Neurobiol Aging 1990;11(1):51-5.
135. Winkler J, Ramirez GA, Kuhn HG, Peterson DA, Day-Lollini PA, Stewart GR, et al. Reversible Schwann cell hyperplasia and sprouting of sensory and sympathetic neurites after intraventricular administration of nerve growth factor. Ann Neurol 1997;41(1):82-93.
136. Jonhagen ME. Nerve growth factor treatment in dementia. Alzheimer Dis Assoc Disord 2000;14 Suppl 1:S31-8.
137. Emerich DF, Winn SR, Harper J, Hammang JP, Baetge EE, Kordower JH. Implants of polymer-encapsulated human NGF-secreting cells in the nonhuman primate: rescue and sprouting of degenerating cholinergic basal forebrain neurons. J Comp Neurol 1994;349(1):148-64.
138. Chen KS, Gage FH. Somatic gene transfer of NGF to the aged brain: behavioral and morphological amelioration. J Neurosci 1995;15(4):2819-25.
139. Tuszynski MH, Roberts J, Senut MC, U HS, Gage FH. Gene therapy in the adult primate brain: intraparenchymal grafts of cells genetically modified to produce nerve growth factor prevent cholinergic neuronal degeneration. Gene Ther 1996;3(4):305-14.
140. Tuszynski MH, Thal L, Pay M, Salmon DP, U HS, Bakay R, et al. A phase 1 clinical trial of nerve growth factor gene therapy for Alzheimer disease. Nat Med 2005;11(5):551-5.
141. Klein RL, Hirko AC, Meyers CA, Grimes JR, Muzyczka N, Meyer EM. NGF gene transfer to intrinsic basal forebrain neurons increases cholinergic cell size and protects from age-related, spatial memory deficits in middle-aged rats. Brain Res 2000;875(1-2):144-51.
142. Blesch A, Conner J, Pfeifer A, Gasmi M, Ramirez A, Britton W, et al. Regulated lentiviral NGF gene transfer controls rescue of medial septal cholinergic neurons. Mol Ther 2005;11(6):916-25.
143. Tuszynski M, Thal L, Pay M, Tong G, Hoi-Sang U, Bakay R, et al. NGF gene therapy. Alzheimer's & Dementia: The Journal of the Alzheimer's Association 2006;2(3):S50.
144. Patel NV, Gordon MN, Connor KE, Good RA, Engelman RW, Mason J, et al. Caloric restriction attenuates Abeta-deposition in Alzheimer transgenic models. Neurobiol Aging 2005;26(7):995-1000.
145. Halagappa VK, Guo Z, Pearson M, Matsuoka Y, Cutler RG, Laferla FM, et al. Intermittent fasting and caloric restriction ameliorate age-related behavioral deficits in the triple-transgenic mouse model of Alzheimer's disease. Neurobiol Dis 2007;26(1):212-20.
146. Lim GP, Calon F, Morihara T, Yang F, Teter B, Ubeda O, et al. A diet enriched with the omega-3 fatty acid docosahexaenoic acid reduces amyloid burden in an aged Alzheimer mouse model. J Neurosci 2005;25(12):3032-40.
147. Vingtdeux V, Dreses-Werringloer U, Zhao H, Davies P, Marambaud P. Therapeutic potential of resveratrol in Alzheimer's disease. BMC Neurosci 2008;9 Suppl 2:S6.
148. Rezai-Zadeh K, Shytle D, Sun N, Mori T, Hou H, Jeanniton D, et al. Green tea epigallocatechin-3-gallate (EGCG) modulates amyloid precursor protein cleavage and reduces cerebral amyloidosis in Alzheimer transgenic mice. J Neurosci 2005;25(38):8807-14.
149. Wang J, Ho L, Zhao Z, Seror I, Humala N, Dickstein DL, et al. Moderate consumption of Cabernet Sauvignon attenuates Abeta neuropathology in a mouse model of Alzheimer's disease. FASEB J 2006;20(13):2313-20.
150. Crouch PJ, White AR, Bush AI. The modulation of metal bio-availability as a therapeutic strategy for the treatment of Alzheimer's disease. FEBS J 2007;274(15):3775-83.

151. Kleihues P, Louis DN, Scheithauer BW, Rorke LB, Reifenberger G, Burger PC, et al. The WHO classification of tumors of the nervous system. J Neuropathol Exp Neurol 2002;61(3):215-25; discussion 226-9.
152. Louis DN, Ohgaki H, Wiestler OD, Cavenee WK, Burger PC, Jouvet A, et al. The 2007 WHO classification of tumours of the central nervous system. Acta Neuropathol 2007;114(2):97-109.
153. Omuro AM, Faivre S, Raymond E. Lessons learned in the development of targeted therapy for malignant gliomas. Mol Cancer Ther 2007;6(7):1909-19.
154. Stupp R, Mason WP, van den Bent MJ, Weller M, Fisher B, Taphoorn MJ, et al. Radiotherapy plus concomitant and adjuvant temozolomide for glioblastoma. N Engl J Med 2005;352(10):987-96.
155. Schaller BJ, Modo M, Buchfelder M. Molecular imaging of brain tumors: a bridge between clinical and molecular medicine? Mol Imaging Biol 2007;9(2):60-71.
156. Ohgaki H, Dessen P, Jourde B, Horstmann S, Nishikawa T, Di Patre PL, et al. Genetic pathways to glioblastoma: a population-based study. Cancer Res 2004;64(19):6892-9.
157. Ohgaki H, Kleihues P. Genetic pathways to primary and secondary glioblastoma. Am J Pathol 2007;170(5):1445-53.
158. Miller CR, Perry A. Glioblastoma. Arch Pathol Lab Med 2007;131(3):397-406.
159. Lang FF, Miller DC, Koslow M, Newcomb EW. Pathways leading to glioblastoma multiforme: a molecular analysis of genetic alterations in 65 astrocytic tumors. J Neurosurg 1994;81(3):427-36.
160. Mellinghoff IK, Wang MY, Vivanco I, Haas-Kogan DA, Zhu S, Dia EQ, et al. Molecular determinants of the response of glioblastomas to EGFR kinase inhibitors. N Engl J Med 2005;353(19):2012-24.
161. Cairncross JG, Ueki K, Zlatescu MC, Lisle DK, Finkelstein DM, Hammond RR, et al. Specific genetic predictors of chemotherapeutic response and survival in patients with anaplastic oligodendrogliomas. J Natl Cancer Inst 1998;90(19):1473-9.
162. Cahill DP, Levine KK, Betensky RA, Codd PJ, Romany CA, Reavie LB, et al. Loss of the mismatch repair protein MSH6 in human glioblastomas is associated with tumor progression during temozolomide treatment. Clin Cancer Res 2007;13(7):2038-45.
163. Hunter C, Smith R, Cahill DP, Stephens P, Stevens C, Teague J, et al. A hypermutation phenotype and somatic MSH6 mutations in recurrent human malignant gliomas after alkylator chemotherapy. Cancer Res 2006;66(8):3987-91.
164. Huse JT, Holland EC. Genetically engineered mouse models of brain cancer and the promise of preclinical testing. Brain Pathol 2009;19(1):132-43.
165. Fomchenko EI, Holland EC. Mouse models of brain tumors and their applications in preclinical trials. Clin Cancer Res 2006;12(18):5288-97.
166. Dai C, Holland EC. Glioma models. Biochim Biophys Acta 2001;1551(1):M19-27.
167. Hu X, Holland EC. Applications of mouse glioma models in preclinical trials. Mutat Res 2005;576(1-2):54-65.
168. Raman V, Pathak AP, Glunde K, Artemov D, Bhujwalla ZM. Magnetic resonance imaging and spectroscopy of transgenic models of cancer. NMR Biomed 2007;20(3):186-99.
169. McConville P, Hambardzumyan D, Moody JB, Leopold WR, Kreger AR, Woolliscroft MJ, et al. Magnetic resonance imaging determination of tumor grade and early response to temozolomide in a genetically engineered mouse model of glioma. Clin Cancer Res 2007;13(10):2897-904.
170. Herholz K, Coope D, Jackson A. Metabolic and molecular imaging in neuro-oncology. Lancet Neurol 2007;6(8):711-24.
171. Leenders WP, Kusters B, Verrijp K, Maass C, Wesseling P, Heerschap A, et al. Antiangiogenic therapy of cerebral melanoma metastases results in sustained tumor progression via vessel co-option. Clin Cancer Res 2004;10(18 Pt 1):6222-30.

172. Leenders W, Kusters B, Pikkemaat J, Wesseling P, Ruiter D, Heerschap A, et al. Vascular endothelial growth factor-A determines detectability of experimental melanoma brain metastasis in GD-DTPA-enhanced MRI. Int J Cancer 2003;105(4):437-43.
173. Claes A, Gambarota G, Hamans B, van Tellingen O, Wesseling P, Maass C, et al. Magnetic resonance imaging-based detection of glial brain tumors in mice after antiangiogenic treatment. Int J Cancer 2008;122(9):1981-6.
174. Veeravagu A, Hou LC, Hsu AR, Cai W, Greve JM, Chen X, et al. The temporal correlation of dynamic contrast-enhanced magnetic resonance imaging with tumor angiogenesis in a murine glioblastoma model. Neurol Res 2008;30(9):952-9.
175. Kauppinen RA. Monitoring cytotoxic tumour treatment response by diffusion magnetic resonance imaging and proton spectroscopy. NMR Biomed 2002;15(1):6-17.
176. Chenevert TL, McKeever PE, Ross BD. Monitoring early response of experimental brain tumors to therapy using diffusion magnetic resonance imaging. Clin Cancer Res 1997;3(9):1457-66.
177. Hollingworth W, Medina LS, Lenkinski RE, Shibata DK, Bernal B, Zurakowski D, et al. A systematic literature review of magnetic resonance spectroscopy for the characterization of brain tumors. AJNR Am J Neuroradiol 2006;27(7):1404-11.
178. Server A, Josefsen R, Kulle B, Maehlen J, Schellhorn T, Gadmar O, et al. Proton magnetic resonance spectroscopy in the distinction of high-grade cerebral gliomas from single metastatic brain tumors. Acta Radiol;51(3):316-25.
179. Hakumaki JM, Poptani H, Sandmair AM, Yla-Herttuala S, Kauppinen RA. 1H MRS detects polyunsaturated fatty acid accumulation during gene therapy of glioma: implications for the in vivo detection of apoptosis. Nat Med 1999;5(11):1323-7.
180. Jacobs AH, Dittmar C, Winkeler A, Garlip G, Heiss WD. Molecular imaging of gliomas. Mol Imaging 2002;1(4):309-35.
181. Jacobs AH, Kracht LW, Gossmann A, Ruger MA, Thomas AV, Thiel A, et al. Imaging in neurooncology. NeuroRx 2005;2(2):333-47.
182. Szeto MD, Chakraborty G, Hadley J, Rockne R, Muzi M, Alvord EC, Jr., et al. Quantitative metrics of net proliferation and invasion link biological aggressiveness assessed by MRI with hypoxia assessed by FMISO-PET in newly diagnosed glioblastomas. Cancer Res 2009;69(10):4502-9.
183. Lyons SK. Advances in imaging mouse tumour models in vivo. J Pathol 2005;205(2):194-205.
184. Rehemtulla A, Stegman LD, Cardozo SJ, Gupta S, Hall DE, Contag CH, et al. Rapid and quantitative assessment of cancer treatment response using in vivo bioluminescence imaging. Neoplasia 2000;2(6):491-5.
185. Szentirmai O, Baker CH, Lin N, Szucs S, Takahashi M, Kiryu S, et al. Noninvasive bioluminescence imaging of luciferase expressing intracranial U87 xenografts: correlation with magnetic resonance imaging determined tumor volume and longitudinal use in assessing tumor growth and antiangiogenic treatment effect. Neurosurgery 2006;58(2):365-72; discussion 365-72.
186. Hsu AR, Cai W, Veeravagu A, Mohamedali KA, Chen K, Kim S, et al. Multimodality molecular imaging of glioblastoma growth inhibition with vasculature-targeting fusion toxin VEGF121/rGel. J Nucl Med 2007;48(3):445-54.
187. Dinca EB, Sarkaria JN, Schroeder MA, Carlson BL, Voicu R, Gupta N, et al. Bioluminescence monitoring of intracranial glioblastoma xenograft: response to primary and salvage temozolomide therapy. J Neurosurg 2007;107(3):610-6.
188. Adams JY, Johnson M, Sato M, Berger F, Gambhir SS, Carey M, et al. Visualization of advanced human prostate cancer lesions in living mice by a targeted gene transfer vector and optical imaging. Nat Med 2002;8(8):891-7.

189. Winkeler A, Sena-Esteves M, Paulis LE, Li H, Waerzeggers Y, Ruckriem B, et al. Switching on the lights for gene therapy. PLoS ONE 2007;2(6):e528.
190. Monfared P, Winkeler A, Klein M, Li H, Klose A, Hoesel M, et al. Noninvasive assessment of E2F-1-mediated transcriptional regulation in vivo. Cancer Res 2008;68(14):5932-40.
191. Neves AA, Brindle KM. Assessing responses to cancer therapy using molecular imaging. Biochim Biophys Acta 2006;1766(2):242-61.
192. Jacobs A, Voges J, Reszka R, Lercher M, Gossmann A, Kracht L, et al. Positron-emission tomography of vector-mediated gene expression in gene therapy for gliomas. Lancet 2001;358(9283):727-9.
193. Voges J, Reszka R, Gossmann A, Dittmar C, Richter R, Garlip G, et al. Imaging-guided convection-enhanced delivery and gene therapy of glioblastoma. Ann Neurol 2003;54(4):479-87.
194. Jacobs AH, Rueger MA, Winkeler A, Li H, Vollmar S, Waerzeggers Y, et al. Imaging-guided gene therapy of experimental gliomas. Cancer Res 2007;67(4):1706-15.
195. Miletic H, Fischer YH, Giroglou T, Rueger MA, Winkeler A, Li H, et al. Normal brain cells contribute to the bystander effect in suicide gene therapy of malignant glioma. Clin Cancer Res 2007;13(22 Pt 1):6761-8.
196. Batchelor TT, Sorensen AG, di Tomaso E, Zhang WT, Duda DG, Cohen KS, et al. AZD2171, a pan-VEGF receptor tyrosine kinase inhibitor, normalizes tumor vasculature and alleviates edema in glioblastoma patients. Cancer Cell 2007;11(1):83-95.
197. Cai W, Chen X. Multimodality imaging of vascular endothelial growth factor and vascular endothelial growth factor receptor expression. Front Biosci 2007;12:4267-79.
198. Cai W, Chen X. Multimodality molecular imaging of tumor angiogenesis. J Nucl Med 2008;49 Suppl 2:113S-28S.
199. Cairns RA, Khokha R, Hill RP. Molecular mechanisms of tumor invasion and metastasis: an integrated view. Curr Mol Med 2003;3(7):659-71.
200. Zhang X, Xiong Z, Wu Y, Cai W, Tseng JR, Gambhir SS, et al. Quantitative PET imaging of tumor integrin alphavbeta3 expression with 18F-FRGD2. J Nucl Med 2006;47(1):113-21.
201. Cao Q, Cai W, Li ZB, Chen K, He L, Li HC, et al. PET imaging of acute and chronic inflammation in living mice. Eur J Nucl Med Mol Imaging 2007;34(11):1832-42.
202. Sipkins DA, Cheresh DA, Kazemi MR, Nevin LM, Bednarski MD, Li KC. Detection of tumor angiogenesis in vivo by alphaVbeta3-targeted magnetic resonance imaging. Nat Med 1998;4(5):623-6.
203. Hsu AR, Hou LC, Veeravagu A, Greve JM, Vogel H, Tse V, et al. In vivo near-infrared fluorescence imaging of integrin alphavbeta3 in an orthotopic glioblastoma model. Mol Imaging Biol 2006;8(6):315-23.
204. Xiong Z, Cheng Z, Zhang X, Patel M, Wu JC, Gambhir SS, et al. Imaging chemically modified adenovirus for targeting tumors expressing integrin alphavbeta3 in living mice with mutant herpes simplex virus type 1 thymidine kinase PET reporter gene. J Nucl Med 2006;47(1):130-9.
205. Arap W, Pasqualini R, Ruoslahti E. Cancer treatment by targeted drug delivery to tumor vasculature in a mouse model. Science 1998;279(5349):377-80.
206. Serganova I, Doubrovin M, Vider J, Ponomarev V, Soghomonyan S, Beresten T, et al. Molecular imaging of temporal dynamics and spatial heterogeneity of hypoxia-inducible factor-1 signal transduction activity in tumors in living mice. Cancer Res 2004;64(17):6101-8.
207. Jacobs A, Dubrovin M, Hewett J, Sena-Esteves M, Tan CW, Slack M, et al. Functional coexpression of HSV-1 thymidine kinase and green fluorescent protein: implications for noninvasive imaging of transgene expression. Neoplasia 1999;1(2):154-61.

208. Loo C, Lowery A, Halas N, West J, Drezek R. Immunotargeted nanoshells for integrated cancer imaging and therapy. Nano Lett 2005;5(4):709-11.
209. Reddy GR, Bhojani MS, McConville P, Moody J, Moffat BA, Hall DE, et al. Vascular targeted nanoparticles for imaging and treatment of brain tumors. Clin Cancer Res 2006;12(22):6677-86.
210. van Tilborg GA, Mulder WJ, Chin PT, Storm G, Reutelingsperger CP, Nicolay K, et al. Annexin A5-conjugated quantum dots with a paramagnetic lipidic coating for the multimodal detection of apoptotic cells. Bioconjug Chem 2006;17(4):865-8.
211. Sosnovik DE, Schellenberger EA, Nahrendorf M, Novikov MS, Matsui T, Dai G, et al. Magnetic resonance imaging of cardiomyocyte apoptosis with a novel magneto-optical nanoparticle. Magn Reson Med 2005;54(3):718-24.
212. Hanahan D, Weinberg RA. The hallmarks of cancer. Cell 2000;100(1):57-70.
213. Laxman B, Hall DE, Bhojani MS, Hamstra DA, Chenevert TL, Ross BD, et al. Noninvasive real-time imaging of apoptosis. Proc Natl Acad Sci U S A 2002;99(26):16551-5.
214. Lee KC, Hamstra DA, Bhojani MS, Khan AP, Ross BD, Rehemtulla A. Noninvasive molecular imaging sheds light on the synergy between 5-fluorouracil and TRAIL/Apo2L for cancer therapy. Clin Cancer Res 2007;13(6):1839-46.
215. Ray P, De A, Patel M, Gambhir SS. Monitoring caspase-3 activation with a multimodality imaging sensor in living subjects. Clin Cancer Res 2008;14(18):5801-9.
216. Coppola JM, Ross BD, Rehemtulla A. Noninvasive imaging of apoptosis and its application in cancer therapeutics. Clin Cancer Res 2008;14(8):2492-501.
217. Messerli SM, Prabhakar S, Tang Y, Shah K, Cortes ML, Murthy V, et al. A novel method for imaging apoptosis using a caspase-1 near-infrared fluorescent probe. Neoplasia 2004;6(2):95-105.
218. Blankenberg FG, Katsikis PD, Tait JF, Davis RE, Naumovski L, Ohtsuki K, et al. In vivo detection and imaging of phosphatidylserine expression during programmed cell death. Proc Natl Acad Sci U S A 1998;95(11):6349-54.
219. Mandl SJ, Mari C, Edinger M, Negrin RS, Tait JF, Contag CH, et al. Multi-modality imaging identifies key times for annexin V imaging as an early predictor of therapeutic outcome. Mol Imaging 2004;3(1):1-8.
220. Zhao M, Beauregard DA, Loizou L, Davletov B, Brindle KM. Non-invasive detection of apoptosis using magnetic resonance imaging and a targeted contrast agent. Nat Med 2001;7(11):1241-4.
221. Petrovsky A, Schellenberger E, Josephson L, Weissleder R, Bogdanov A, Jr. Near-infrared fluorescent imaging of tumor apoptosis. Cancer Res 2003;63(8):1936-42.
222. Schellenberger EA, Bogdanov A, Jr., Petrovsky A, Ntziachristos V, Weissleder R, Josephson L. Optical imaging of apoptosis as a biomarker of tumor response to chemotherapy. Neoplasia 2003;5(3):187-92.
223. Chang J, Ormerod M, Powles TJ, Allred DC, Ashley SE, Dowsett M. Apoptosis and proliferation as predictors of chemotherapy response in patients with breast carcinoma. Cancer 2000;89(11):2145-52.
224. Brekke C, Williams SC, Price J, Thorsen F, Modo M. Cellular multiparametric MRI of neural stem cell therapy in a rat glioma model. Neuroimage 2007;37(3):769-82.
225. Aboody KS, Brown A, Rainov NG, Bower KA, Liu S, Yang W, et al. Neural stem cells display extensive tropism for pathology in adult brain: evidence from intracranial gliomas. Proc Natl Acad Sci U S A 2000;97(23):12846-51.
226. Benedetti S, Pirola B, Pollo B, Magrassi L, Bruzzone MG, Rigamonti D, et al. Gene therapy of experimental brain tumors using neural progenitor cells. Nat Med 2000;6(4):447-50.

227. Ehtesham M, Kabos P, Kabosova A, Neuman T, Black KL, Yu JS. The use of interleukin 12-secreting neural stem cells for the treatment of intracranial glioma. Cancer Res 2002;62(20):5657-63.
228. Ehtesham M, Kabos P, Gutierrez MA, Chung NH, Griffith TS, Black KL, et al. Induction of glioblastoma apoptosis using neural stem cell-mediated delivery of tumor necrosis factor-related apoptosis-inducing ligand. Cancer Res 2002;62(24):7170-4.
229. Barresi V, Belluardo N, Sipione S, Mudo G, Cattaneo E, Condorelli DF. Transplantation of prodrug-converting neural progenitor cells for brain tumor therapy. Cancer Gene Ther 2003;10(5):396-402.
230. Shah K, Bureau E, Kim DE, Yang K, Tang Y, Weissleder R, et al. Glioma therapy and real-time imaging of neural precursor cell migration and tumor regression. Ann Neurol 2005;57(1):34-41.
231. Staflin K, Honeth G, Kalliomaki S, Kjellman C, Edvardsen K, Lindvall M. Neural progenitor cell lines inhibit rat tumor growth in vivo. Cancer Res 2004;64(15):5347-54.
232. Noble M, Dietrich J. Intersections between neurobiology and oncology: tumor origin, treatment and repair of treatment-associated damage. Trends Neurosci 2002;25(2):103-7.
233. Miletic H, Fischer Y, Litwak S, Giroglou T, Waerzeggers Y, Winkeler A, et al. Bystander killing of malignant glioma by bone marrow-derived tumor-infiltrating progenitor cells expressing a suicide gene. Mol Ther 2007;15(7):1373-81.
234. Bulte JW, Kraitchman DL. Monitoring cell therapy using iron oxide MR contrast agents. Curr Pharm Biotechnol 2004;5(6):567-84.
235. Modo M, Hoehn M, Bulte JW. Cellular MR imaging. Mol Imaging 2005;4(3):143-64.
236. Zhang Z, Jiang Q, Jiang F, Ding G, Zhang R, Wang L, et al. In vivo magnetic resonance imaging tracks adult neural progenitor cell targeting of brain tumor. Neuroimage 2004;23(1):281-7.
237. Anderson SA, Glod J, Arbab AS, Noel M, Ashari P, Fine HA, et al. Noninvasive MR imaging of magnetically labeled stem cells to directly identify neovasculature in a glioma model. Blood 2005;105(1):420-5.
238. Arbab AS, Pandit SD, Anderson SA, Yocum GT, Bur M, Frenkel V, et al. Magnetic resonance imaging and confocal microscopy studies of magnetically labeled endothelial progenitor cells trafficking to sites of tumor angiogenesis. Stem Cells 2006;24(3):671-8.
239. Fulci G, Breymann L, Gianni D, Kurozomi K, Rhee SS, Yu J, et al. Cyclophosphamide enhances glioma virotherapy by inhibiting innate immune responses. Proc Natl Acad Sci U S A 2006;103(34):12873-8.
240. Waerzeggers Y, Klein M, Miletic H, Himmelreich U, Li H, Monfared P, et al. Multimodal imaging of neural progenitor cell fate in rodents. Mol Imaging 2008;7(2):77-91.

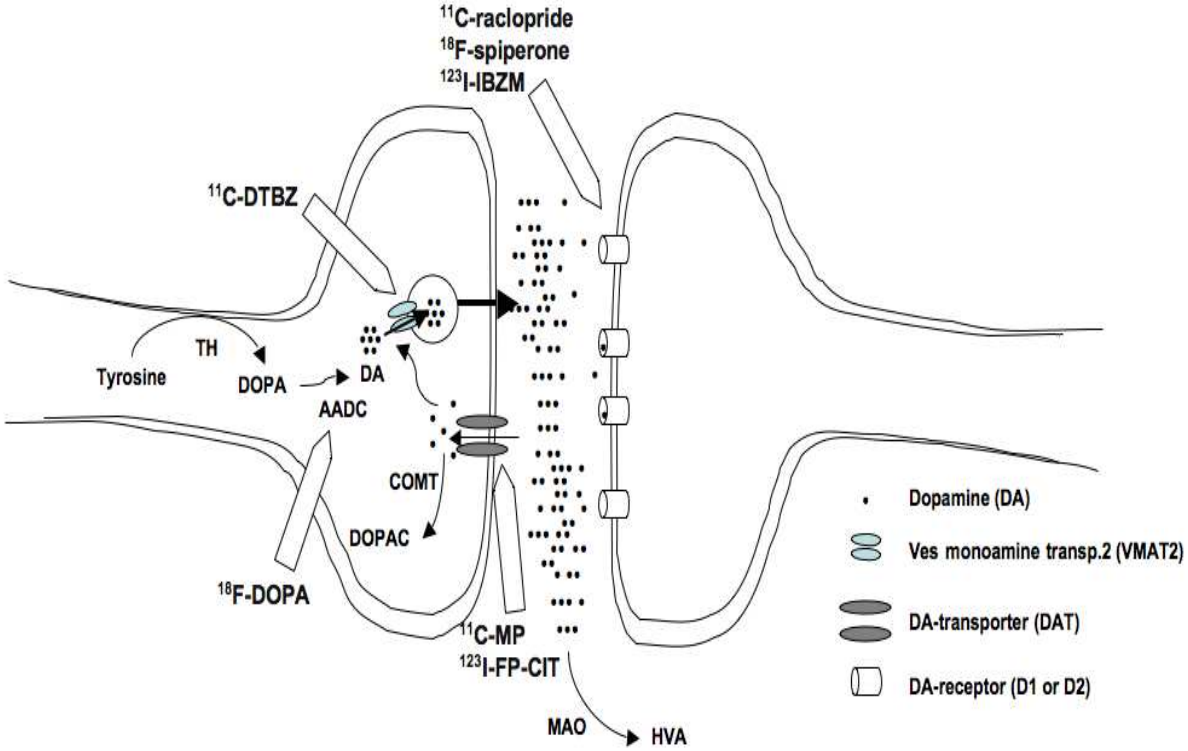

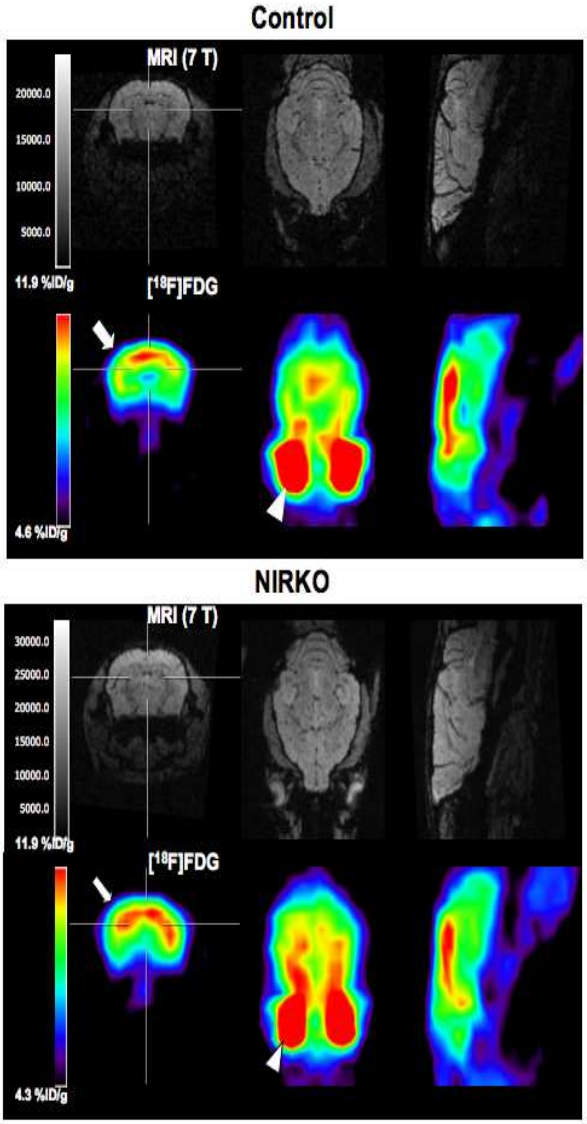

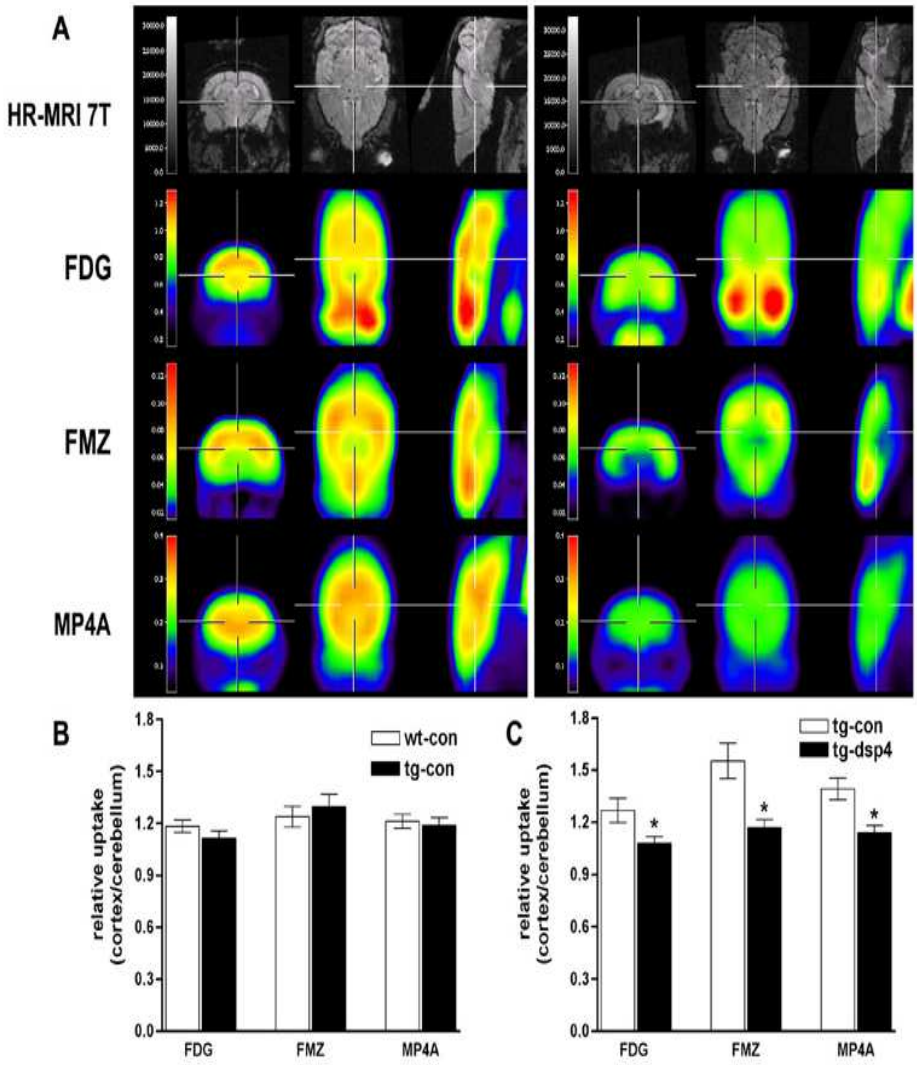
A
HR-MRI 7T
FDG
FMZ
MP4A
B
wt-con
tg-con
relative uptake
(cortex/cerebellum)
1.8
1.5
1.2
0.9
0.6
0.3
0.0
FDG
FMZ
MP4A
C
tg-con
tg-dsp4
relative uptake
(cortex/cerebellum)
*
*
*
FDG
FMZ
MP4A

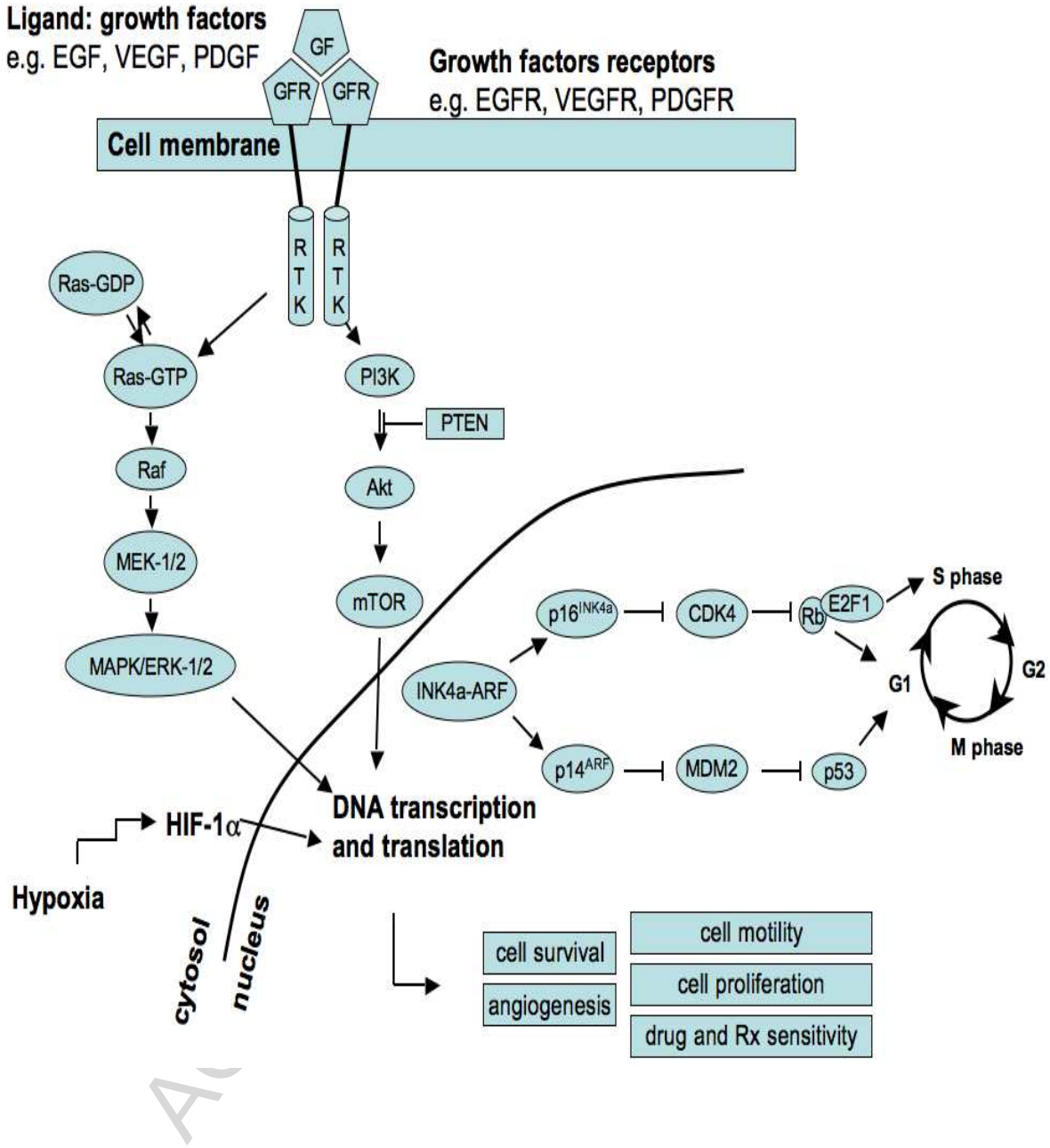

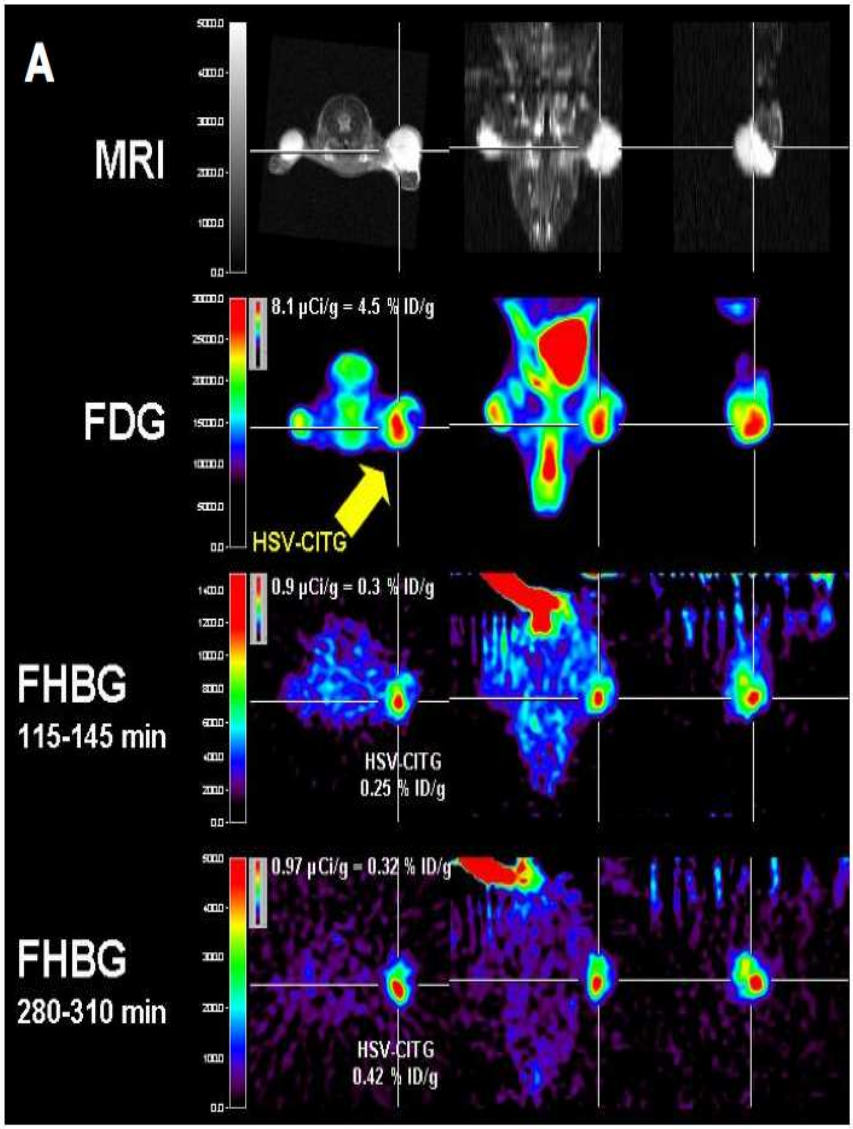

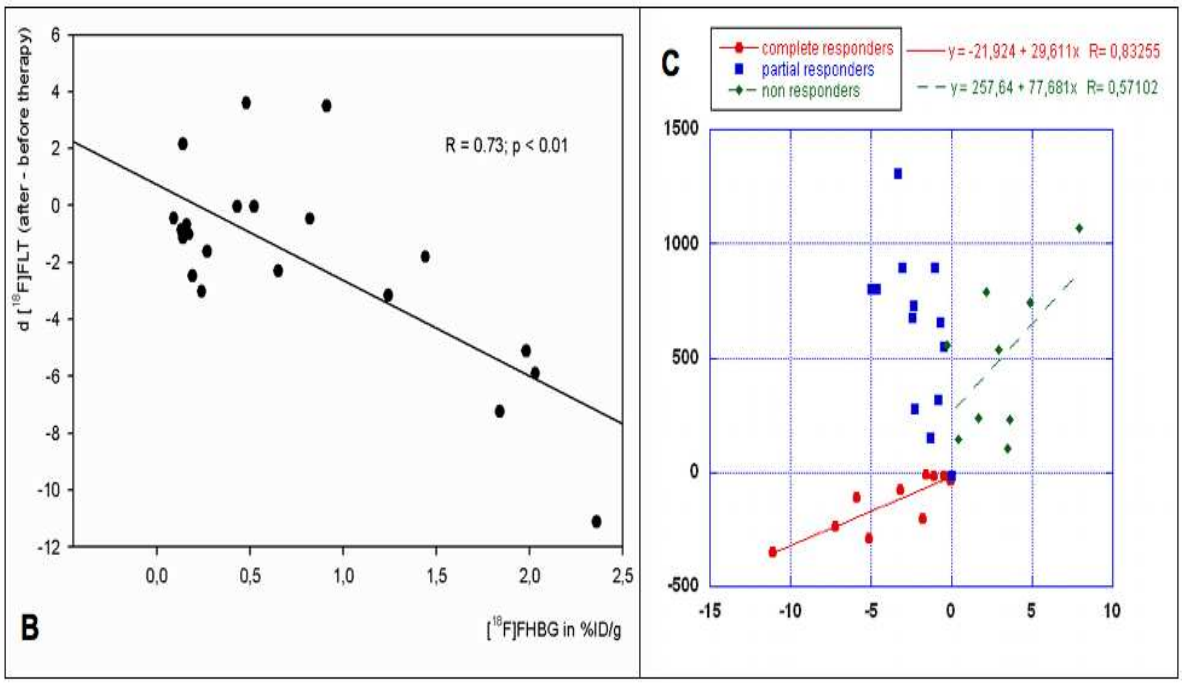

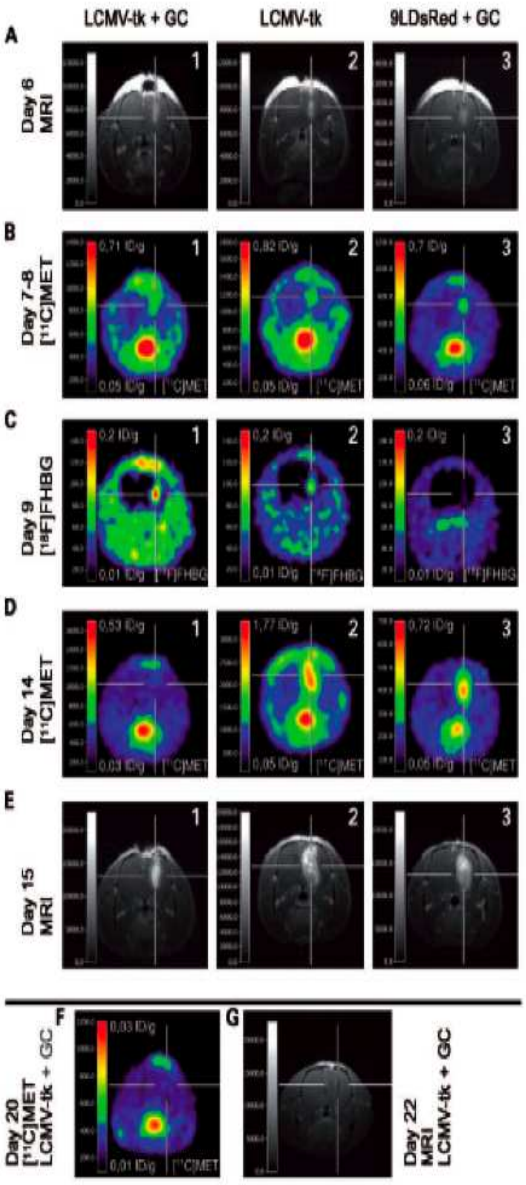

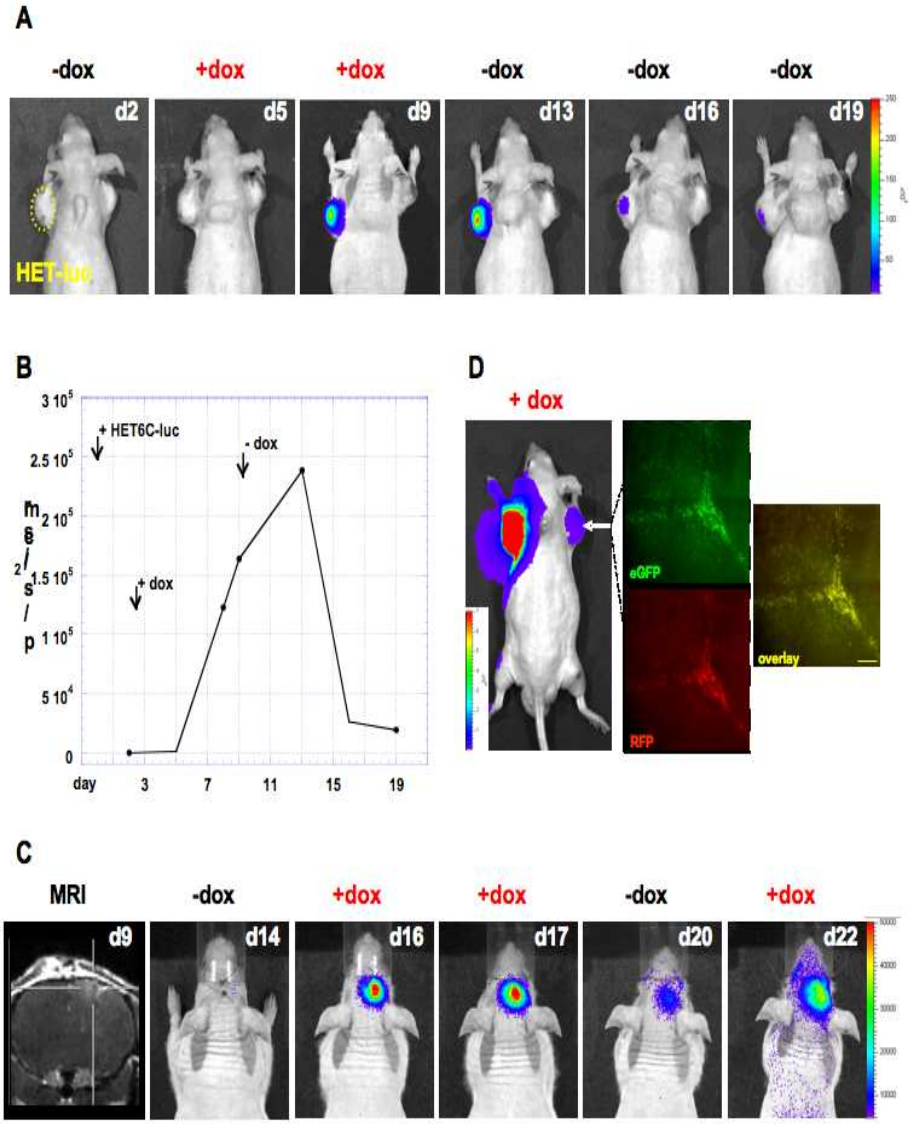
A
-dox
+dox
+dox
-dox
-dox
-dox
d2
d5
d9
d13
d16
d19
HET-luc
B
+ HET6C-luc
- dox
+ dox
day
3
7
11
15
19
D
+ dox
eGFP
RFP
overlay
C
MRI
-dox
+dox
+dox
-dox
+dox
d9
d14
d16
d17
d20
d22

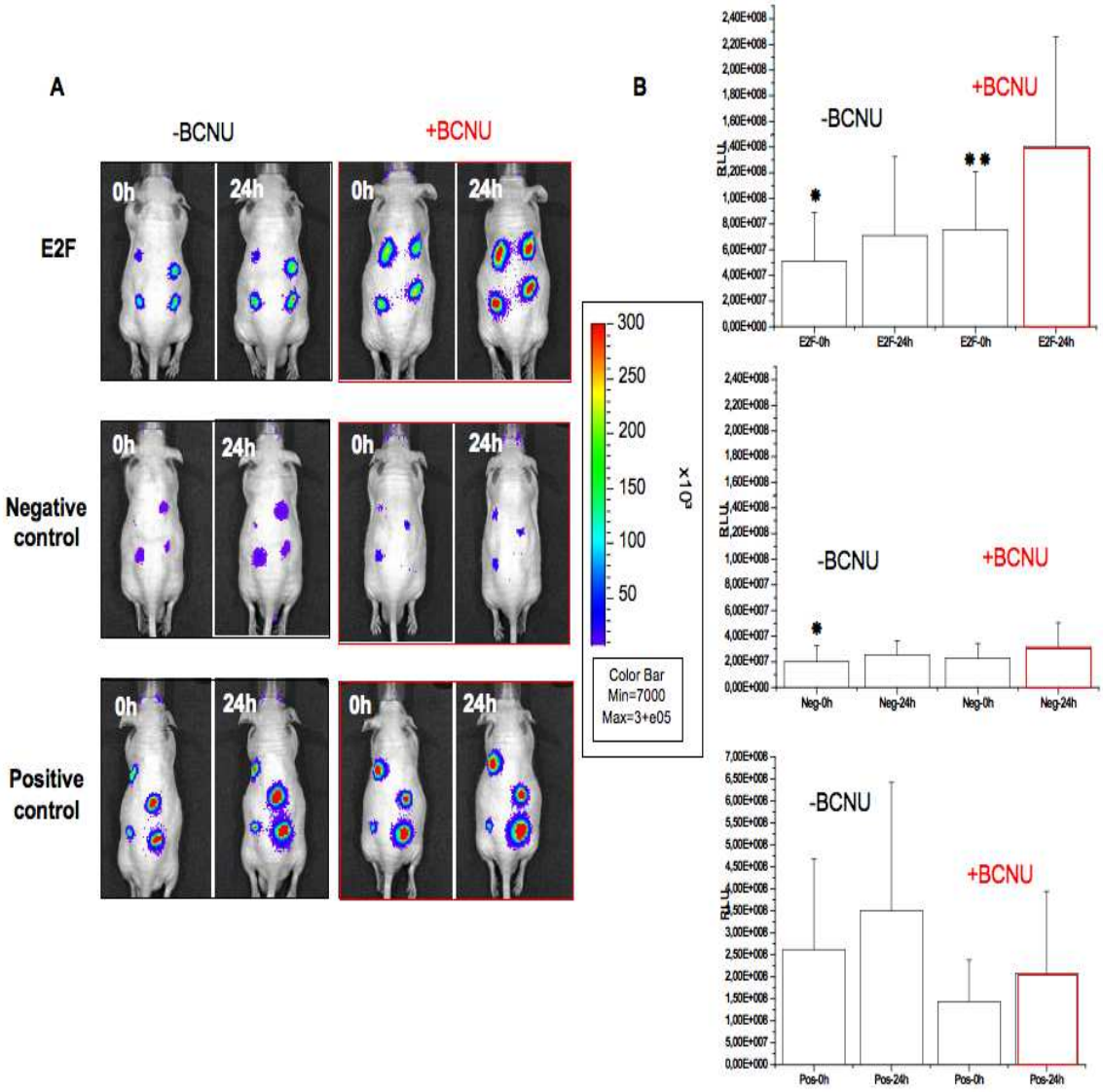
A
-BCNU
+BCNU
E2F
Negative control
Positive control
0h
24h
300
250
200
150
100
50
x10³
Color Bar
Min=7000
Max=3+e05
B
-BCNU
+BCNU
R.L.U.
E2F-0h
E2F-24h
Neg-0h
Neg-24h
Pos-0h
Pos-24h